Global Biogeochemical Cycles

RESEARCH ARTICLE
10.1029/2018GB006047

Estimating Air-Sea Carbon Flux Uncertainty Over the Tropical Pacific: Importance of Winds and Wind Analysis Uncertainty

A. M. Chiodi[1,2], **J. P. Dunne**[3], **and D. E. Harrison**[2]

[1]Joint Institute for the Study of the Atmosphere and Ocean, University of Washington, Seattle, WA, USA, [2]Pacific Marine Environmental Laboratory, National Oceanic and Atmospheric Administration, Seattle, WA, USA, [3]Geophysical Fluid Dynamics Laboratory, National Oceanic and Atmospheric Administration, Princeton, NJ, USA

Key Points:
- Mooring data highlight the importance of accurate wind knowledge for understanding tropical Pacific air-sea carbon flux variability
- Analysis product winds used in previous basin-scale carbon flux study exhibit significant differences in mean, variability, and trend
- The mooring array winds are critical to identifying wind product limitations to characterizing long-term trends in air-sea carbon flux

Correspondence to:
A. M. Chiodi,
andy.chiodi@noaa.gov

Citation:
Chiodi, A. M., Dunne, J. P., & Harrison, D. E. (2019). Estimating air-sea carbon flux uncertainty over the tropical Pacific: Importance of winds and wind analysis uncertainty. *Global Biogeochemical Cycles*, *33*. https://doi.org/10.1029/2018GB006047

Received 3 AUG 2018
Accepted 29 DEC 2018
Accepted article online 5 JAN 2019

Abstract The tropical Pacific is a major natural source of CO_2 to the atmosphere and contributor to global air-sea carbon flux variability. High time-resolution wind and CO_2 measurements from equatorial Pacific moorings reveal the primary factor controlling mooring-observed flux variability to be near-surface wind variability, above CO_2 variability, in this region over the last 10 years. The analysis product winds used most widely in previous calculations of basin-scale carbon flux are compared with mooring winds and found to exhibit significant differences in mean, variability, and trend. Earth system model calculations are in basic agreement with the mooring results and used to estimate effects of wind uncertainty on our knowledge of regional air-sea carbon exchange. Results show that NCEP1 and NCEP2 winds contain biases large enough to obscure the interannual variability of CO_2 flux (RMSE $\approx \sigma$) and cause spurious 25-year (1992–2016) trend components in equatorial Pacific carbon flux of 0.038–0.039 and 0.016–0.021 Pg C yr^{-1} per decade, respectively. These spurious trends act to reduce by up to 50% the 25-year trend in equatorial Pacific carbon flux simulated by the Earth system model under increasing atmospheric CO_2 concentration. The Cross-Calibrated-Multi-Platform wind product tracks observed variability of equatorial Pacific wind better (interannual RMSE $\approx 0.4\sigma$) than the NCEP reanalyses when site sampled at mooring locations yet still causes a spurious regional trend (0.03 Pg C yr^{-1} per decade) that masks 40% of the simulated 25-year trend in carbon flux. The mooring observations are fundamental to identifying the limitations of current wind products to characterizing long-term trends and understanding air-sea carbon exchange.

Plain Language Summary The tropical Pacific Ocean stands out as a significant natural source of carbon to the atmosphere—even rivaling U.S. emissions. Knowing how this source has changed over recent decades and how it might change in coming decades is important to understanding and predicting net oceanic carbon uptake. Estimates of the effect that changes in the wind have had on regional air-sea carbon exchange depend strongly on the wind analysis used. Direct wind observations from the array of approximately 70 moored buoys spanning the tropical Pacific are critical to our ability to monitor the system for long-term trend.

1. Introduction

The variability in space and time of the air-sea flux of carbon dioxide (CO_2) is an important part of the coupled climate-carbon system. Of particular interest are the extent to which the net oceanic carbon uptake has changed over recent years and how it might change in coming decades. At present, the net oceanic uptake is estimated to be about 2.4 Pg C yr^{-1} or 25% of the carbon emissions from fossil fuel burning and industrial activity (Le Quéré et al., 2018; carbon budget). The extent to which different regions contribute is also of interest. Uptake of carbon through the ocean surface is thought to occur largely over the Southern Ocean (south of 35°S), with substantial contribution also from the North Pacific and North Atlantic in boreal winter (Takahashi et al., 2009). The tropical Pacific, wherein relatively carbon-rich water is brought to the surface through upwelling in the equatorial region and along the South American coast, is known to provide a counteracting source of carbon to the atmosphere. Equatorial Pacific carbon flux has been estimated to be near +0.5 Pg C yr^{-1} (positive = upward) by Takahashi et al. (2009) and +0.4 Pg C yr^{-1} by Ishii et al. (2014), contributions that equate to approximately one third of recent U.S. emissions from fossil fuels, which was estimated as 1.4 Pg C yr^{-1} over 2014 by Boden et al. (2017).

One challenge confronting assessment of long-term carbon uptake is interannual variability. The tropical Pacific has been estimated to have large interannual variability of air-sea carbon flux that is thought to contribute substantially to the global interannual variability of air-sea carbon flux (Feely et al., 2002, 2006; Park et al., 2010). Global interannual surface flux variability was estimated recently to have had a standard deviation of 0.2 Pg C yr^{-1} over the period 1990–2009 by Wanninkhof et al. (2013) and 0.31 Pg C yr^{-1} over 1992–2009 by Rödenbeck et al. (2015). The uptake of carbon by the ocean is also thought to have increased over recent decades, but the estimated magnitude of increase varies widely depending on the method used to estimate it. For example, Wanninkhof et al. (2013) reported decadal ocean uptake increases that ranged by a factor of 4, from 0.13 to 0.5 Pg C yr^{-1} per decade, depending on the methodological approach across forced biogeochemical ocean model simulations of air-sea carbon flux, inference of air-sea carbon flux based on observed interior ocean carbon inventories and forced ocean model-simulated ocean circulations (a.k.a. ocean inversions), atmospheric inversions based on atmospheric circulation estimates and measured atmospheric carbon concentrations, and empirical estimation of air-sea carbon flux based on measurements of surface ocean and near-surface atmospheric carbon concentrations and wind.

Our ability to estimate air-sea carbon flux has benefited greatly from progress made over recent decades in collection of oceanic carbon observations from ships of opportunity, research vessels, moorings, and drifting buoys. Unfortunately, the available direct observations of carbon concentrations in most regions of the global ocean remain sparse in space and time (Bakker et al., 2016). Estimating global air-sea carbon flux from the available ocean surface carbon observations currently requires synthesizing basin-wide near-surface ocean CO_2 concentration or partial pressure (pCO_{2sw}) fields based on the available carbon data and other sources of information, including statistical relationships between pCO_{2sw} and other surface marine variables that are more widely measured (e.g., most of the pCO2 products discussed by Rödenbeck et al., 2015). Approaches focusing on the relationship between sea surface temperature and pCO_{2sw} variability have been developed and used now for several decades to estimate basin-wide surface ocean pCO_2 variability in the tropical Pacific as inferred through the surface temperature variability (e.g., Feely et al., 2006; Park et al., 2010). Full-field estimation of air-sea carbon flux also requires gap-filling synthesis of the available measurements of the atmospheric partial pressure of CO_2 (pCO_{2a}). Estimating the time-varying zonal mean of pCO_{2a} from available land surface, land tower, aircraft, and ship pCO_{2a} sampling (GLOBALVIEW-CO2, 2011), as well as atmospheric inversion techniques (e.g., Rödenbeck et al., 2015), have been used to produce gap-filled gridded pCO_{2a} fields.

Where the necessary carbon observations or syntheses are available, air-sea carbon flux (F) is commonly estimated using the bulk formula:

$$F = k \times K_S \times \Delta pCO_2, \tag{1}$$

so that F is dependent on ΔpCO_2, the interfacial difference between the partial pressure (or fugacity, which is similar to partial pressure but corrects for gas nonideality) of CO_2 in the near-surface seawater and overlying air ($\Delta pCO_2 = pCO_{2sw} - pCO_{2a}$); K_s, the temperature and salinity-dependent solubility of CO_2, which is popularly calculated based on the formulation of Weiss (1974); and the gas transfer velocity (k), a.k.a. piston velocity, thought to depend upon wind stress and associated near-surface turbulence, ocean waves, and bubble injection, surface-surfactant conditions, as well as temperature and near-surface humidity (Blomquist et al., 2017; Nightingale et al., 2000; Wanninkhof et al., 2013, and references therein). Because wind variability plays a role in driving the relevant changes in many of these contributing variables (e.g., turbulence and bubble injection) and is much more widely measured than several of the other variables (e.g., bubble injection and surface surfactants), the gas transfer velocity, k, has typically been parameterized as a function of near-surface wind speed, with linear (Smethie et al., 1985), piecewise linear (Liss & Merlivat, 1986), combination linear-quadratic (e.g., Nightingale et al., 2000), quadratic (e.g., Ho et al., 2006; Wanninkhof et al., 2013), and cubic (McGillis et al., 2001) forms all having been suggested and used previously (see Boutin et al., 2002, and Otero et al., 2013, for regional comparisons). Recent studies of basin-scale carbon flux (e.g., Ishii et al., 2014; Park et al., 2010; Rödenbeck et al., 2015; Takahashi et al., 2009; Wanninkhof et al., 2013) have tended to parameterize gas transfer velocity using the form

$$k = k_{660} \times U^{p} \times (660/Sc)^{n}, \quad (2)$$

wherein k_{660} is constant over space and time, n is assumed to be 0.5 (Wanninkhof, 1992), p is assumed to equal 2 (quadratic wind speed dependence), and U^2 is the square of wind speed at 10-m height. Typically, U^2 is calculated based on measurements of U (mean wind speed) obtained over some averaging interval. The wind-time-averaging scales used in previous carbon flux studies range from climatological long-term averages (e.g., Wanninkhof, 1992), in which case other sources of information must be relied upon to adjust for the nonlinear effects of unresolved U variability on U^2, down to wind measurements over a few minutes or less (e.g., Fassbender et al., 2017; Ho et al., 2006; Sutton et al., 2017; Wanninkhof, 2014), in which case it has been determined or assumed that no such nonlinear adjustment is needed. The value 660 corresponds to the Schmidt number of CO_2 in seawater. Although the $n = 0.5$ Schmidt number term $(660/Sc)^{0.5}$ in equation (2) and CO_2 solubility (K_s) term in equation (1) vary substantially with temperature, the product $(660/Sc)^{0.5} \times K_s$ that results when equation (2) is used in equation (1) with $n = 0.5$ is relatively insensitive to temperature change. For example, the climatological sea surface temperature range in the eastern equatorial Pacific, which varies from approximately 22 °C in boreal autumn to 27 °C in spring, produces changes in K_s of ~12%, but only <1% in the product $(660/Sc)^{-0.5} \times K_s$. Thus, the primary potential sources of variability in the commonly used quadratic air-sea carbon flux parameterization (F in equation (1), with $p = 2$ and $n = 0.5$ in equation (2)) are the square of near-surface wind speed (U^2) and the near-surface ocean-to-air partial pressure (or fugacity) difference of CO_2 (ΔpCO_2).

Direct measurements of air-sea carbon flux based on the eddy-covariance approach (Blomquist et al., 2017; see also McGillis et al., 2001) found that using the parameters $k_{660} = 0.96$ and $p = 1.68$ in equation (2) provided the best fit to their eddy-covariance flux measurements made in 10-m wind speeds ranging from ~2 to 25 m/s in the North Atlantic. These eddy-covariance results showed substantial spread at a given wind speed, however, which may be attributable to gas flux dependencies on factors other than wind speed and methodological uncertainties. Parameterizations based on direct flux measurements such as these serve as a reminder of the uncertainties involved in parameterizing k as a function of wind speed. A more common approach has been to infer k_{660} based on knowledge of global winds, the time history of atmospheric bomb-C_{14} gas concentration, and the rate of change of the oceanic concentration (e.g., Naegler, 2009; Sweeney et al., 2007; Wanninkhof, 1992, 2014; Wanninkhof et al., 2013). Dedicated dual tracer experiments, such as the $^3HE/SF_6$ injection experiments described by Ho et al. (2006; see also Nightingale et al., 2000), provide another means of estimating k as a function of wind speed. Recently, Roobaert et al. (2018) examined the effects of adjusting k_{660} according to the analysis product used for wind information such that the product $k_{660} \times U^2$ retained a similar global and time mean among different wind analyses. Roobaert et al. (2018) found substantial uncertainty in regional air-sea carbon flux remained over the equatorial Pacific, North Atlantic, and Southern Ocean even after making these adjustments, demonstrating the importance of accurate wind knowledge for estimating flux over these regions. Among the more recent dual-tracer and C_{14}-based studies, the value decided upon for k_{660} varies somewhat (e.g., Ho et al., 2006 suggest $k_{660} = 2.79 \pm 0.02$; Wanninkhof, 2014; Wanninkhof et al., 2013, report a best fit of $k_{660} = 2.51$), but the $p = 2$ assumption is used in each case.

To apply the flux parameterization described by equations (1) and (2) to estimate basin-scale air-sea carbon flux variability (or to use the bomb-C_{14} approach to deduce k_{660}), accurate knowledge of U^2 over the global ocean is required. Direct wind measurements in the marine boundary layer are available from ships and moored buoys. Wind speeds have been remotely sensed by satellite-based scatterometer and radiometer instruments over the past several decades. Complete direct measurement of the surface wind field across the globe, however, remains—like complete pCO_2 sampling—a goal for the future. The task of producing a full wind field over the ocean surface thus depends upon synthesizing the available measurements, or subsets of these measurements, into full wind fields, that is, gap filling across space and time. Numerical weather models run in data assimilation mode have become a popular means to produce full, regularly gridded wind fields. These *reanalysis* products provide wind fields on subdaily timescales (most products used in recent carbon exchange studies have 6-hr resolution) and have been commonly used in contemporary carbon flux studies. For example, Rödenbeck et al. (2015) used the winds produced by the NCEP/NCAR Reanalysis 1 (*NCEP1* hereafter) and Takahashi et al. (2009) and Park et al. (2010) used the modified NCEP-DOE Reanalysis 2 (*NCEP2* hereafter) for knowledge of global wind variability.

To understand the uncertainties with flux calculations like these, it is important to characterize the limitations of analyzed wind products (Bates & Merlivat, 2001; Wallcraft et al., 2009). Comparison with high-quality direct measurements of wind speed and direction offers a basis for doing this. Chiodi and Harrison (2017a, 2017b), for example, looked in detail at how well the wind and wind stress information contained in the NCEP1 and NCEP2 reanalyses agreed with the observations provided by the tropical Pacific moored buoy array (a.k.a. TAO/TRITON), which spans the equatorial Pacific with buoy spacing set to match the observed zonal and meridional coherence length scales of the winds (Harrison & Luther, 1990). They found substantial biases in NCEP1, NCEP2, and the more recent ERA-Interim (Dee et al., 2011) reanalysis wind products over this region.

In addition to reanalysis wind products like NCEP1, NCEP2, and ERA-Interim, the Cross-Calibration Multi-Platform (CCMP; Atlas et al., 2011) wind product has also been used in global carbon studies (e.g., Wanninkhof, 2014; Wanninkhof et al., 2013; Wanninkhof & Triñanes, 2017; Ishii et al., 2014). The CCMP product assimilates mooring and satellite-based estimates of near-surface winds, which are derived from measurements of backscattered microwave radiation over the ocean surface. Direct measurement of winds coincident in time and space with the backscatter signal is necessary for calibrating the satellite backscatter to estimates of vector winds. The CCMP product also depends on a *first-guess* or background wind field. In the first CCMP version (CCMP1), the NCEP2 near-surface wind product was used as background information for assimilation of the available satellite winds. In the second version (CCMP2), ERA-Interim, which itself assimilates many of the satellite products used in the CCMP approach, was used. The mean and trend biases in the tropical Pacific winds in CCMP1 and CCMP2 were evaluated relative to the daily averaged TAO/TRITON wind observations by McGregor et al. (2017) and found to depend on the choice of background wind field. CCMP, like NCEP1 and NCEP2, is available on a 6-hr time grid, which was suggested by Wanninkhof (2014), in consideration of the CCMP case, to be sufficiently high in resolution to resolve the timescales of wind variability relevant to the nonlinear U dependence of the bulk gas flux parameterization (equation (1)).

Ocean general circulation models that include carbon chemistry along with basic upper ocean biology (e.g., phytoplankton, zooplankton, detritus, and nutrient interaction) have also been developed to simulate the coupled interaction between ocean physics and biogeochemical processes when forced with information about the surface exchanges of heat, momentum, fresh water, gases, and nutrients (or some combination thereof). The simulation of air-sea carbon flux in ocean biogeochemical models typically uses the same form of gas flux parameterization described above (e.g., Orr et al., 2017) and is therefore also reliant on near-surface atmospheric pCO_2 and wind speed. This atmospheric information has been prescribed based on observational syntheses in forced biogeochemical ocean simulation experiments (e.g., Aumont & Bopp, 2006; Doney et al., 2009; Le Quéré et al., 2010; McKinley et al., 2004; Sarmiento et al., 2010) and, alternatively, by coupling biogeochemical ocean models to atmosphere, sea ice, and land-carbon models in state-of-the-art Earth System Models (ESMs; e.g., Dunne et al., 2012, 2013; Lovenduski et al., 2016; Law et al., 2017). Models offer dynamically consistent sets of wind and ΔpCO_2 fields and can be useful for interpreting and synthesizing observations and understanding the processes controlling observed carbon system variability. Models are only approximations, however, and must be evaluated against accurate observations on relevant space and time scales before their relevance to real-world processes can be assessed.

Fortunately, for more than a decade, surface moorings in the equatorial Pacific have supplied the accurate observations of wind and the carbon system to compute the various terms in equations (1) and (2) directly. Because of the coverage and duration of observation of air-sea carbon flux from the equatorial Pacific, as well as its substantial influence on global levels of air-sea carbon flux and flux variability, we focus here on examining the impacts that uncertainty in our knowledge of the winds has on our ability to estimate air-sea CO_2 flux from this region and assess control by ΔpCO_2 and wind on the measured flux variability in the equatorial Pacific.

In addition to the direct measurements of pCO_2 from seven moorings located in the equatorial Pacific, we also exploit winds measured by the full tropical Pacific mooring array to better understand wind uncertainty impacts on regional carbon flux. This array is composed of nearly 70 moorings spanning the basin from 137°E to 95°W and 8° or 9°N to 8°S. The winds from the mooring array can be used to assess the mean, variability, and 25-year trend biases in the commonly used analyzed wind products. To estimate the impacts that

Table 1
Start Month of MAPCO2 pCO_2 Measurements Along With the Number of Days of Finalized 3-Hourly ΔpCO_2 Data Available Used in This Study

MAPCO2 site	Start	Days
Papa (145°W, 50°N)	Jul 2007	1,773
KEO (145°E, 32°N)	Sep 2007	1,925
WHOTS (158°W, 23°N)	Jun 2007	1,847
TAO 165°E, 8°S	Jun 2009	751
TAO 165°E, 0°N	Feb 2010	396
TAO 170°W, 0°N	Jul 2005	1,500
TAO 155°W, 0°N	Jun 2005	704
TAO 140°W, 0°N	May 2004	1,883
TAO 125°W, 0°N	Mar 2005	2,106
TAO 110°W, 0°N	Sep 2009	1,066
Stratus (85°W, 20°S)	Oct 2006	2,517

these regional wind uncertainties and biases have on our ability to determine regional air-sea carbon flux and flux variability, we additionally exploit the pCO_2 fields simulated by an ESM integrated with realistically increasing atmospheric CO_2 concentration that reproduces 1992–2016 average equatorial Pacific air-sea CO_2 flux within the range of observation-based estimates listed above (0.4–0.5 Pg C yr^{-1}). Our results reveal substantial biases among the analyzed product winds and resultant fluxes and highlight the importance that the mooring winds play in identifying and potentially constraining wind uncertainty effects on air-sea carbon flux over this highly wind-sensitive region.

2. Data Sets and Methods

2.1. Carbon Moorings

Surface seawater and near-surface atmospheric pCO_2 measurements in the equatorial Pacific were provided by seven moorings equipped with autonomous pCO_2 (MAPCO2, 2017; Sutton et al., 2014) systems that make 3-hourly measurements of near-sea surface (~0.5-m depth) and atmospheric (~1.5 m above surface) mole fractions of CO_2, along with sea surface temperature, salinity, and sea level pressure (last accessed April 2018). Data from four other MAPCO2 systems deployed in the Pacific but outside of the equatorial regions (see Fassbender et al., 2017; Sutton et al., 2017) were also analyzed to offer an observational point of comparison to the rather unique air-sea CO_2 flux behavior observed over the equatorial Pacific (as discussed in section 3.1). The start date (range 2004–2010) and amount of the MAPCO2 pCO_2 measurements used depend on the availability at each site and are summarized in Table 1.

2.2. Moored Buoy Winds

Our main source of observational wind information over the equatorial Pacific is provided by the tropical Pacific moored buoy array (TAO, 1992), which consists of ~70 buoys (only a small subset is currently MAPCO2-equipped) spanning the width of the Pacific Ocean basin with 10°–15° longitude spacing in the east-west direction and 2°–3° latitude spacing in the north-south direction from 8°S to 8° or 9°N. This spacing was designed to match the observed coherence scales of equatorial Pacific wind variability on multiday and longer timescales, meaning that the array provides adequate knowledge of the regional wind variability when all or nearly all buoys are reporting (Luther & Harrison, 1984). Based on forced ocean model experiments over the 1992–2011 period, Chiodi and Harrison (2017a) confirmed that this observing system design works as it was designed for providing wind knowledge necessary to adequately simulate the observed sea surface temperature anomaly development associated with the development of El Niño-Southern Oscillation events. Data return from the array first reached 60% over the Pacific Ocean waveguide in 1992, which is the first year of moored wind observations used herein. Moorings typically measure winds at 3.5 to 4 m above the sea surface. Thus, either they or the 10-m wind estimates produced by the reanalyses and satellite analyses must be adjusted in height to facilitate cross-platform comparison. Here we adjusted the mooring winds to 10-m height assuming neutral atmospheric stability (as also done in Sutton et al., 2017) and using a logarithmic height adjustment approach (as in Mears et al., 2001), which equates, in the case of typical 4-m mooring wind measurements and 1.52×10^{-4}-m oceanic surface roughness length (Peixoto & Oort, 1992), to multiplying the mooring wind speed observations by 1.09 (a 9% increase adjusting from 4- to 10-m winds).

We also analyzed mooring winds from the TAO/Triton subset of observations adjusted to 10-m height based on the COARE 3.0b parameterization (Cronin et al., 2006; Fairall et al., 2003) made available by the TAO Project office at www.pmel.noaa.gov/tao/oceansites/flux/main.html. We have compared 10-m wind speed squared based on each of these two approaches and found similar results (e.g., time-averaged wind speed squared at 140°W, 0°N differs by <0.01%). While we expect 10-m wind speeds from the TAO/Triton observations and COARE 3.0b parameterization to also provide accurate information when available, there are considerable gaps in the COARE case caused by the absence of the other meteorological observations necessary for implementing COARE 3.0b. For this reason, we herein rely on TAO/Triton wind observations and the logarithmic adjustment listed above for 10-m wind information.

For the comparisons discussed below, in order to estimate gas transfer velocity, we first calculated wind speed squared (U^2) values from the available high-frequency wind speed observations provided by the buoys. The high-frequency averaging interval is 10 min for the buoys including and east of the 165°E line and 1 hr for the buoys farther west (the TRITON part of the array). We then averaged these high-frequency U^2 values onto the time grid of the respective companion time series (3-hr MAPCO2 ΔpCO_2 observations or 6-hr analysis product winds). For the mooring observations, we use the k_{660} value of 2.71, suggested by Ho et al. (2006) and previously used for mooring flux estimation by Fassbender et al. (2017). The Wanninkhof et al. (2013) value of 2.51 could be chosen instead without qualitatively affecting our results; for example, the change in the 1992–2016 mean and 25-year trend in regional CO_2 flux contributed by a given data set's wind biases would remain the same, as a fraction of the total unbiased amount, regardless of which k_{660} value was used.

2.3. Analyzed Wind Products

We also use surface wind estimates from two numerical weather models run in data assimilation mode, as well as a pair (versions 1 and 2) of satellite reanalysis wind products. These are the NCEP/NCAR Reanalysis 1 (NCEP1:, 1996) described by Kalnay et al. (1996; 6-hourly and 2.5° latitude × 2.5° longitude resolution), the NCEP-DOE Reanalysis 2 (NCEP2:, 2002) described by Kanamitsu et al. (2002; 6-hourly and 2.5° × 2.5° resolution), and the CCMP satellite reanalysis wind synthesis described by Atlas et al. (2011; 6-hourly and 0.25° × 0.25° resolution). CCMP's version 1 (CCMP1, 2017) used NCEP2 for background wind information and is available only until 2011. CCMP version 2 (CCMP2, 2017) uses ERA-Interim 10-m winds as background and is available over our full study period (1992–2016 for wind observations). Wind speed squared (U^2) information was calculated from the NCEP1, NCEP2, CCMP1, and CCMP2 6-hourly averaged near-surface winds, which are nominally representative of the wind conditions at 10-m height. We chose these products for consideration here based on their recent use in large-scale carbon flux studies (as described in section 1).

We calculate comparison statistics between the mooring winds and the analysis product wind fields using two methods whose 25-year trend characteristics we compare in section 6. In the first method, the analyzed wind fields were subsampled at each buoy site using linear interpolation in the meridional and zonal direction from the four reanalysis grid point values nearest the location of the buoy. This method mimics the effect of imaginarily placing buoys in the reanalysis field. This method is referred to as buoy site sampling, hereafter, and has similarly been referred to as spot sampling previously (Wanninkhof & Triñanes, 2017). In the second method, we sample the analyzed wind fields by averaging them over rectangular regions drawn around the available buoy locations, with zonal and meridional bounds spaced equidistant from adjacent buoy locations, that is, averaging over boxes spanning 2°–3° in the meridional and 10°–15° in the zonal direction. This method is referred to as the buoy box-averaging method.

2.4. Earth System Model Data

Simulated fields of pCO_{2a}, pCO_{2sw}, U^2, and air-sea carbon flux were obtained from NOAA's Geophysical Fluid Dynamics Laboratory (GFDL) ESM 2G (2017), a state-of-the-art coupled carbon-climate Earth System Model (Dunne et al., 2012, 2013), which participated in the CMIP5 project (Taylor et al., 2012). As employed here, ESM 2G is integrated with a prognostic atmospheric CO_2 tracer restored with an annual timescale at all atmospheric levels to the preindustrial reference value of 286 ppmv during the model spin-up and then to historical (1861–2005) and RCP8.5 Scenario (2006–2100) forcing for CMIP5 (Taylor et al., 2012).This relatively gentle annual restoring allows the prognostic atmospheric CO_2 to retain atmospheric pCO_2 regional and temporal variability on subannual timescales for comparability to observational timescales.

The ocean component, Generalized Ocean Layer Dynamics (Hallberg, 1995), uses a 1° horizontal grid increasing to ⅓° meridionally at the equator, and 63 vertical levels, including two mixed layers (Hallberg, 2003; Thompson et al., 2003), two buffer layers, and 59 interior layers. The ocean biogeochemical and ecological component is Tracers of Ocean Phytoplankton with Allometric Zooplankton code version 2.0 (TOPAZ2; Dunne et al., 2010; Henson et al., 2009) with 30 tracers representing various biogeochemical cycles, including carbon, nitrogen, phosphorus, alkalinity, iron, and surface sediment $CaCO_3$ (Dunne et al., 2012). Carbon is cycled through the atmosphere, ocean, and land in GFDL-ESM 2G. TOPAZ2 includes three explicit phytoplankton groups with modified growth physiology (Geider et al., 1997) and size-based

relationship of production and loss (Dunne et al., 2005). Alkalinity and dissolved inorganic carbon are initialized from the Global Ocean Data Analysis Project (Key et al., 2004). The air-sea carbon flux, ΔpCO_2, and wind speed from the model are calculated initially from 3-hourly model output and then saved at daily resolution to facilitate the analyses described in sections 3 and 4. The modeled wind speed squared, in terms of its buoy-sampled average over the equatorial Pacific (~40 m^2/s^2) and spatial structure of the mean across the equatorial Pacific, including enhancements over the easterly trade wind regime in the central equatorial Pacific (not shown for brevity), is qualitatively consistent with TAO/Triton observations, which exhibit a regional and time mean of ~44 m^2/s^2.

3. Results

3.1. Wind Versus ΔpCO_2 Control on Flux Variability

The air-sea carbon partial pressure difference (ΔpCO_2) and the wind speed squared (U^2) term in the commonly used quadratic bulk CO_2 flux parameterization (equations (1) and (2)) are the primary candidates for driving variability in air-sea CO_2 flux. We begin by examining the MAPCO2 carbon and mooring wind observations for the relative extent to which changes in the observed ΔpCO_2 and U^2 time series control the variability of air-sea CO_2 flux at each MAPCO2 site. To evaluate the relative ΔpCO_2 and U^2 controls on flux variability, we examine the RMSE between our base-case calculation of the flux (based on 3-hourly observations of ΔpCO_2 and high-frequency U^2 observations) and component calculations of flux variability performed alternately with U^2 or ΔpCO_2 terms constant at their study period mean. Primary control over the flux variability by one or the other of these variables is thereby revealed when the RMSE produced by omitting one (dominant) component of variability substantially exceeds the RMSE produced by omitting the variability contributed by omitting the other (secondary) component. Stated alternatively, if the variability of the calculated flux does not change much even after one of these variables is replaced by its time mean, then that component contributes little flux variability.

Figure 1 illustrates this situation for the case of the MAPCO2-equipped mooring at 125°W, 0°N. This site offers approximately 13,500 3-hourly pairs of direct pCO_2 and wind observations over the study period (~40% data return, period 2005–2016) and is located in the heart of the upwelling-influenced cold-tongue region of the equatorial Pacific.

The CO_2 flux estimated by direct wind and carbon observations at this site remained positive (net CO_2 transport from ocean to atmosphere) over all times for which data are available and has a mean over the period shown of 8.3×10^{-8} mol · m^{-2} s^{-1}. To highlight variability at subseasonal and longer timescales, the flux is shown in this case at monthly averaged resolution (black curves in Figure 1). Over the September–October 2009 and 2012 portions of the time series shown in Figure 1, the high-frequency (10-min) wind data were not available even though daily averaged wind data were available. Rather than leave these two portions of the figure blank, we filled them with the result of calculating CO_2 flux based on the available daily average winds after adjusting for the effects of neglecting the subdaily contribution to U^2. This adjustment was estimated based on the average difference between U^2 calculated from daily and high-frequency winds over the adjacent years for which they were both available and equated to increasing the flux based on daily averaged winds by 5.4%. This was done for illustrative purposes. The mooring-based calculation results described hereafter are all based on the available high-frequency wind observations.

The monthly averaged flux standard deviation at this site is 2.8×10^{-8} mol · m^{-2} s^{-1}. Recalculating the monthly averaged flux after removing the carbon system variability (i.e., holding ΔpCO_2 constant; light green curve in Figure 1 upper panel) introduces an RMSE in flux that is half as large as the standard deviation of the base case shown in Figure 1. We repeated this calculation using daily, rather than monthly, averages of flux and found qualitatively similar results; although the base-case flux standard deviation is substantially larger at a daily (4.2×10^{-8} mol · m^{-2} s^{-1}) than monthly timescale, reflecting the considerable amount of flux variability revealed at synoptic and shorter timescales by the MAPCO2 systems, the error introduced by holding ΔpCO_2 constant increases proportionally moving from monthly to daily averages such that the RMSE to standard deviation ratio is nearly the same regardless of whether daily or monthly averages are used (RMSE/σ = 0.50 and 0.51, respectively in this case). Discrepancies between the constant-carbon and base-case flux time series are evident in each year for which there are observations

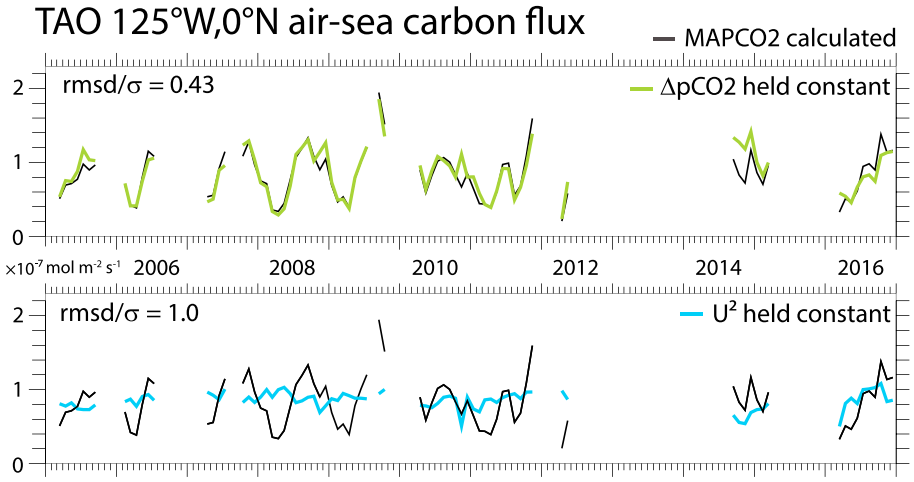

Figure 1. Monthly averaged air-sea carbon flux based on the available 3-hourly mooring observations of ΔpCO_2 and winds at 125°W, 0°N (black curves). Positive values indicate a source of CO_2 to the atmosphere (net flux is from sea to air). Upper panel shows the result of holding ΔpCO_2 constant at its mean (i.e., removing effects of carbon variability) in light green: Most of the variability seen in the raw case remains intact in this case. Lower panel shows the result of holding U^2 constant (removing effects of wind variability) in light blue. In this case the amplitude of the error introduced equals that of the actual signal. Wind speed provides the main control on CO_2 flux at this site, over the directly observed period.

available (cf. black and light green curves in upper panel of Figure 1). These discrepancies highlight intervals in which ΔpCO_2 variability contributes to air-sea carbon flux at this site. The base-case flux variability, however, is approximated with useful accuracy even after the carbon system variability has been removed: ΔpCO_2 is not the main source of observed flux variability at this location.

On the other hand, removing wind variability effects by holding U^2 constant at its mean produces a RMSE that equals the base-case flux standard deviation (RMSE/$\sigma \sim 1$ for both the daily and monthly averaged case). The air-sea carbon flux variability at this site is dominated by variability in the near-surface winds over the time for which the observations are available.

To quantify the relative control of wind and carbon variability on CO_2 flux, we introduce a flux variability metric (R_{fv}) defined as the ratio of the wind speed squared-associated RMSE ($RMSE_U$) and carbon partial pressure differential-associated RMSE ($RMSE_C$):

$$R_{fv} = RMSE_U / RMSE_C.$$

Values of R_{fv} near unity signify balanced control of the flux variability between carbon and wind contributions, whereas values substantially greater than 1 indicate primary control by the wind speed squared and values substantially lower than 1 by the carbon partial pressure differential. For the case presented in Figure 1, R_{fv} based on monthly averaged time series (as shown) is 2.3. R_{fv} based on daily averages of flux (not shown for figure clarity) is qualitatively similar (2.1), indicating wind control on flux variability in either case.

R_{fv} values for each of the seven other equatorial Pacific MAPCO2 equipped buoys, as well as four moorings outside of the equatorial region, were computed based on daily averaged flux time series (themselves calculated based on 10-min winds and 3-hourly pCO_2 values) and illustrated by filled circles in Figure 1. Daily rather than monthly averages of carbon flux were used in this case because gaps in the records from some of these moorings prohibit many full monthly averages from being calculated (especially 165°E, 0°N). Comparison of the equatorial and nonequatorial mooring results reveals a basic pattern characterized by primarily wind-controlled flux variability in the equatorial, and especially central equatorial region, but generally stronger carbon control of the flux variability outside of the equatorial region.

We also calculated R_{fv} based on the simulation of U^2, ΔpCO_2, and air-sea CO_2 flux from ESM 2G (field shown in Figure 2). We used daily averages of the simulated time series in this case, which we sampled

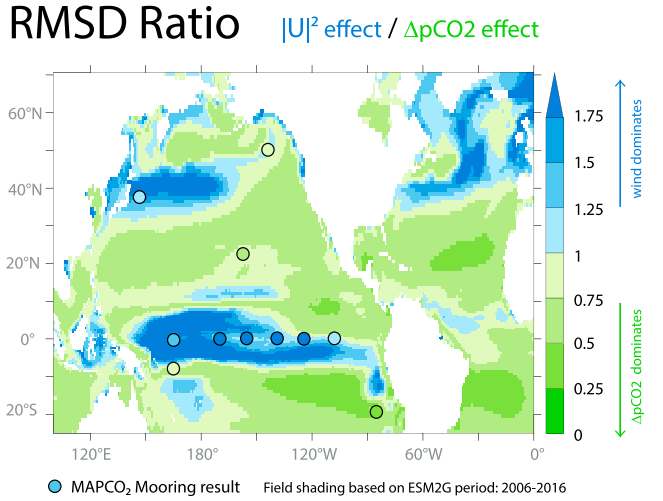

Figure 2. The ratio of the RMSE introduced by holding U^2 constant in the bulk parametrization calculation of air-sea carbon flux, over the RMSE introduced by holding ΔpCO_2 constant. Filled circles show results based on MAPCO2 carbon and mooring wind observations. Broader field shows results based on GFDL's ESM 2G.

over a period chosen to match that over which the direct observations are available (2006–2016). The ESM results are in semiquantitative agreement with the available mooring results. Both sets of results agree that wind variability mainly controls the flux variability over most of the equatorial Pacific. Outside of the equatorial region, the MAPCO2 results reveal R_{fv} values ranging from nearly 1.0 to 0.49, and the model results match the character (i.e., degree to which they are above, near, or below unity) of the mooring results.

3.2. Wind Speed Uncertainty Effects on CO_2 Flux at the MAPCO2 Buoy Sites

Results from the previous section highlight the importance of having accurate knowledge of both near-surface wind and pCO_2 to accurately estimate and understand equatorial Pacific CO_2 flux variability. In this section, we examine the biases introduced in daily averaged air-sea CO_2 flux variability when the buoy-observed winds are substituted for winds site sampled from the analyzed wind products that have most commonly been used in recent carbon flux studies (NCEP1, NCEP2, and CCMP; in this case we use CCMP2 because CCMP1 is not available past 2011).

The noise-to-signal ratios associated with replacing the buoy winds with site-sampled (i.e., mimicking observations from an imaginary buoy placed in the reanalysis wind field) analysis product winds are listed in Table 2 for each of the 11 Pacific mooring sites considered. The *noise* metric used in this case is the RMSE in carbon flux produced by substituting in the analysis product winds for the base-case mooring winds. The *signal* metric is the standard deviation of the base-case flux time series (σ). To produce the values listed in Table 2, the analyses winds were interpolated from their native 6-hourly resolution to the 3-hourly MAPCO2 time grid to calculate fluxes. Then RMSE/σ was calculated based on the respective (mooring and analysis-based) daily averaged carbon flux.

Comparison of the equatorial (TAO) moorings with those located elsewhere in the Pacific reveals that the relative impacts of the uncertainty associated with the analysis winds on flux are, on average, larger in the equatorial region than elsewhere. For example, the mean noise-to-signal ratio produced by substituting-in NCEP2 U^2 information is 0.81 averaged over the seven TAO-MAPCO2 moorings but about one third less (0.53) averaged over the four nonequatorial Pacific moorings. This difference is statistically significant at the 99% confidence interval based on Monte Carlo subsampling, with replacement, of the respective TAO and non-TAO values in the NCEP2 column of Table 2. This equatorial to nonequatorial difference is even more striking based on the other two wind products, with CCMP2 introducing equatorial region errors that are roughly twice, and NCEP1 3 times as large as the nonequatorial errors. This relatively high sensitivity to wind uncertainty over the equatorial region is consistent with the findings from section 3.1 that identified wind variability as the main control on the flux variability over this region.

The uncertainties associated with the three wind products considered, however, differ substantially from one another. In the NCEP1 and NCEP2 cases, the noise introduced at each equatorial mooring site approaches the signal (RMSE/σ near 1). We repeated this calculation after averaging the respective flux time series to monthly mean resolution and confirmed that noise to signal remains qualitatively similar (signal-to-noise ratio = 1) over the equatorial region using NCEP1 or NCEP2. CCMP2 (at daily or monthly resolution) offers a substantially improved noise-to-signal ratio relative to these two reanalyses.

Table 2
Noise-to-Signal (RMSD/σ) Ratios and Mean Differences in Air-Sea Carbon Flux Caused by Substituting the Respective Analysis Product Winds for Those Measured by the Moored Buoys and Recalculating the Flux

Wind product	CCMP v2	NCEP2	NCEP1
MAPCO2 Site	Noise-to-signal ratio (mean difference)		
Papa (145°W, 50°N)	0.16 (+5%)	**0.79** (+42%)	0.37 (+5%)
KEO (145°E, 32°N)	0.24 (+6%)	**0.66** (+20%)	0.47 (−13%)
WHOTS (158°W, 23°N)	0.10 (+4%)	0.34 (−22%)	0.38 (−28%)
TAO 165°E, 8°S	0.34 (+2%)	**0.58** (+10%)	0.51 (−8%)
TAO 165°E, 0°N	0.25 (−7%)	**1.1** (−27%)	1.3 (−35%)
TAO 170°W, 0°N	0.20 (−7%)	**0.60** (−17%)	0.65 (−25%)
TAO 155°W, 0°N	0.36 (−5%)	**0.80** (−19%)	0.92 (−31%)
TAO 140°W, 0°N	0.24 (−4%)	**0.83** (−15%)	1.04 (−37%)
TAO 125°W, 0°N	0.45 (−5%)	**0.81** (−4%)	0.98 (−37%)
TAO 110°W, 0°N	0.27 (−5%)	**0.94** (+11%)	0.98 (−25%)
Stratus (85°W, 20°S)	0.09 (−4%)	0.31 (+10%)	0.28 (+11%)

Note. The RMSD and time series standard deviation (σ) are based on daily averages. RMSD/σ values >0.5 are highlighted in bold type. Mean differences are listed as percentage change relative to the mean mooring-based carbon flux. Negative changes (lower flux amplitudes) are listed in red type.

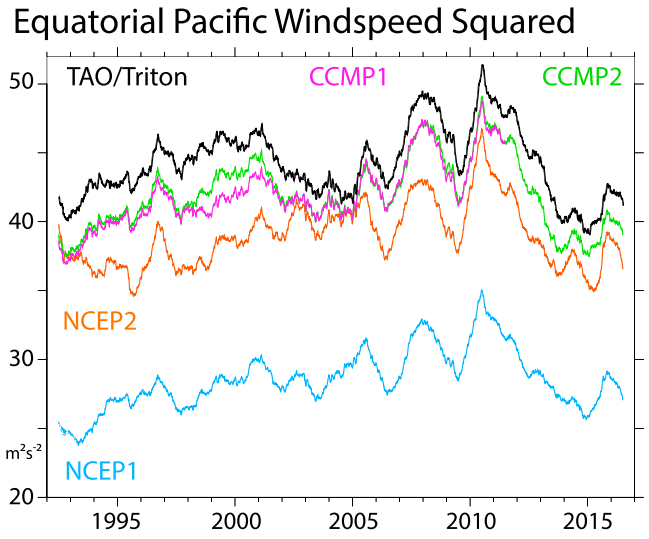

Figure 3. Ten-meter wind speed squared averaged spatially over all available equatorial Pacific moored buoy observations, and smoothed with a 365-day running mean filter to highlight annual and longer timescale variability (black line). Also shown are the corresponding buoy site-sampled results from four analyzed wind products: CCMP1 (pink line), CCMP2 (green line), NCEP2 (orange line), and NCEP1 (blue line).

We also calculated the mean flux offsets produced by substituting the analyzed wind products for the mooring winds and found a similar qualitative difference between the CCMP2 and reanalysis winds. Whereas the CCMP2 mean offsets over the equatorial Pacific ranged from being 4% to 7% different from the mooring wind results, the reanalysis products are characterized by larger equatorial region offsets, near 20% in the NCEP2 and 35% in the NCEP1 case. Interestingly, the three products all tended to exhibit negative offsets (U^2 less than observed) over the equatorial region, even though different biases were seen outside of this region. Evidently, for analyzed wind products like these, the bias characteristics revealed by direct observation in one region cannot be assumed to hold elsewhere.

In sections 4 and 5, we make use of the rest of the tropical Pacific moored buoy array (including the majority of moored buoys that are not MAPCO2 equipped) along with the ΔpCO_2 fields provided by ESM 2G, to offer an expanded analysis of the effects that biases in the analyzed wind products have on our ability to estimate and monitor the magnitude, interannual variability, and trend in equatorial Pacific CO_2 flux.

4. Wind Analysis Uncertainty Assessed With the Full Tropical Pacific Moored Buoy Array

In this section we use the high-frequency wind observations from the full tropical Pacific moored buoy array (~70 buoys spanning the width of the basin) to quantify the basin-wide biases in U^2 contained in the analysis wind products over the period 1992–2016. The buoy array first reached >60% complete data return over the core Pacific waveguide in 1992, with respect to the full deployment configuration shown in Figure 3. Biases between the mooring winds and analyzed product winds are calculated in this section based on site sampling the analysis winds when and where the high-frequency buoy winds are available over this period.

To highlight the differences between the buoy observations and analysis winds that are evident across the region on interannual and longer time scales, we have averaged the analyzed product biases in space (across all buoys) and then applied a 365-day running mean filter to this region-averaged time series. The resulting annually averaged U^2 time series are shown in Figure 3 as absolute values and in Figure 4 with their time means removed. The absolute value case reveals that there are substantial regional differences in wind speed squared between the mooring winds and the analyzed products, with the moorings recording the highest values of the four data sets. The spatial distribution of the time-mean offset is explored below.

Discrepancies between the variability of equatorial Pacific U^2 observed by the buoys and contained in the NCEP2 and NCEP1 reanalyses are large enough to obscure the behavior of the actual system on interannual and longer time scales: The RMSE between the mooring and NCEP2 U^2 annual-and-regionally averaged time series (red and black lines in Figure 4) is 70% as large as the standard deviation of the observed variability (black line); that is, the noise is large enough to substantially obscure the actual variability of the system. This ratio is comparably large (58%) in the NCEP1 case. Differences in the character of the buoy-observed and analyzed-product wind variability are evident throughout the study period but are especially large in the several years bracketing the turn of the century.

There is also a large discrepancy in the trend of U^2 measured by the buoys and contained in the reanalyses. Gauged by the slope of the best fit line, the mooring winds exhibit a small 25-year trend in U^2 ($0.029\ m^2 \cdot s^{-2}\ yr^{-1}$), whereas the trends based on NCEP2 and NCEP1 are 4 to 5 times larger than this (0.11 and $0.15\ m^2 \cdot s^{-2}\ yr^{-1}$, respectively). Using Student's t metric for trend statistical significance, the trend bias in the NCEP1 case is large enough that a statistically significant trend would be misleadingly identified at the 90% confidence interval (effective time between independent samples estimated as 900 days based on Leith's, 1973 method; see Harrison & Chiodi, 2015 for trend statistical significance discussion) although the trend based on the mooring winds is much smaller and not statistically different from zero.

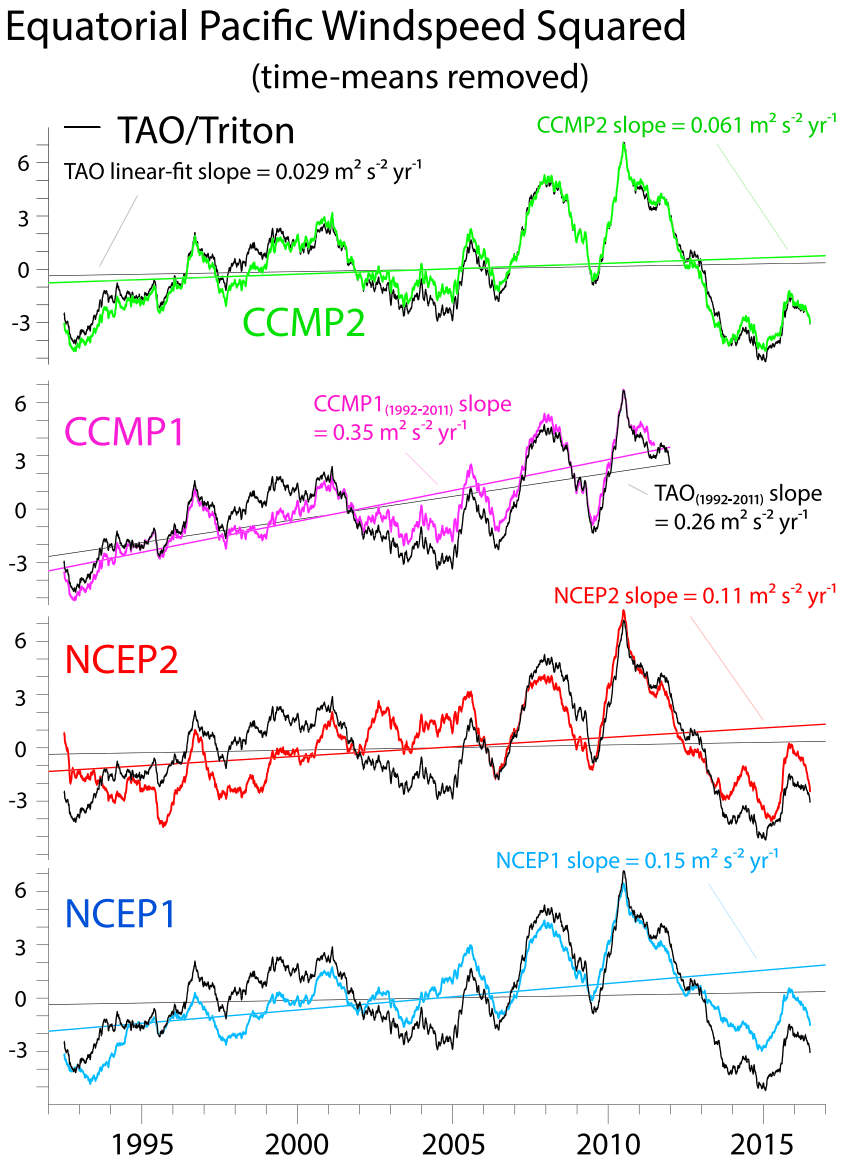

Figure 4. The same site-sampled wind speed squared time series shown in Figure 3, except with their time means removed. Straight lines show the respective least squares fits. The time series are plotted such that the *x* axis values represent the center date of the corresponding 365-day averaging period.

After accounting for their difference in means, the CCMP1 result (Figure 4, pink line) tracks the buoy result much more closely than the reanalyses. Discrepancies, however, are still evident at subannual timescales that lead to a less than ideal noise-to-signal ratio (RMSE/σ_{obs} = 0.39) in the CCMP1 case. The largest multi-year offsets are evident in the 1997–2006 interval and have the same character as the NCEP2 offsets during this time. One possible explanation for this is that the use of the NCEP2 winds as background information for the CCMP1 satellite-wind assimilation technique substantially influences the outcome during this interval (cf. McGregor et al., 2017).

The CCMP2 anomalies (green line in Figure 4) track the mooring winds more closely than the other three products considered and accordingly has the smallest interannual noise-to-signal ratio (RMSE/σ_{obs} = 0.21) of the four wind analysis cases considered here. However, there is still a spurious trend component in CCMP2 that causes its 25-year trend (slope of best fit line = 0.061 $m^2 \cdot s^{-2} \cdot year^{-1}$) to exceed the buoy result by a factor of 2.

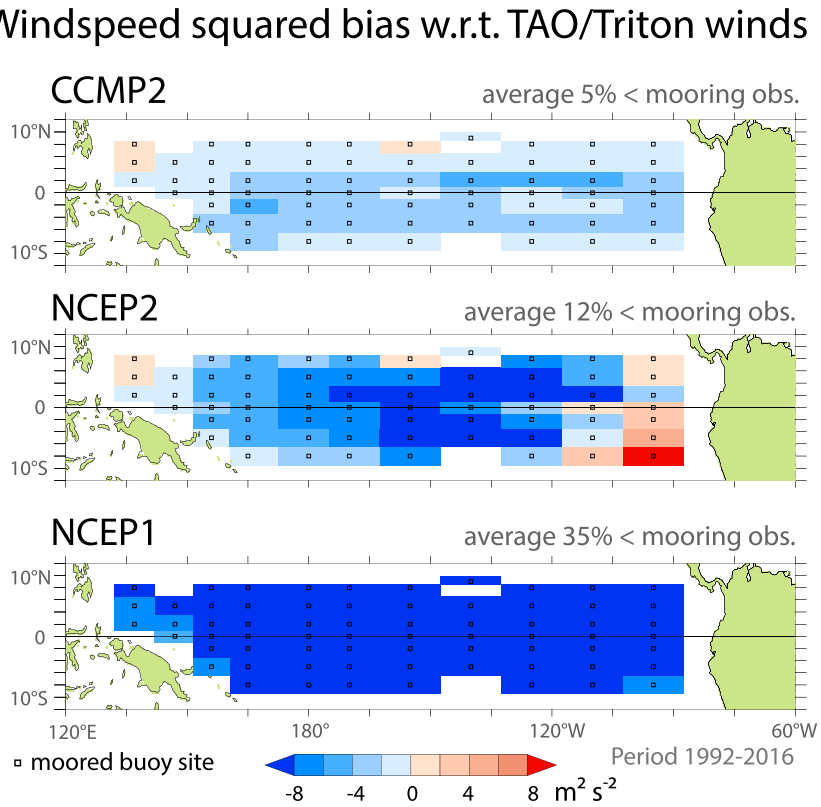

Figure 5. Mean offsets between the TAO/TRITON mooring-observed wind speed squared values and the buoy-sampled analysis wind products that span the 1992–2016 study period.

The spatial distribution of time-mean offsets between U^2 calculated from the high-frequency mooring winds and analysis product winds is illustrated by buoy location in Figure 5 for the analysis products available over the full study period (NCEP1, NCEP2, and CCMP2). The all-buoy and all-time averaged difference between the buoy-observed and analysis-sampled U^2 is negative (observed U^2 higher than analysis result) in each case, with the average analysis product U^2 magnitude ranging from 5% (CCMP2) to 35% (NCEP1) less than the mooring observed value. The NCEP2 result, at 12% less than observed, offers improvement over the NCEP1 result in this case. The CCMP2 result (5% less) is even closer to the observed value, based on this site-sampled comparison approach.

Interestingly, the mean offsets between the buoy and analysis-derived U^2 time series are not uniform across the basin but change character depending on location and chosen analysis product. For example, although the equatorial basin-wide mean bias is negative in each case, larger than observed U^2 values are still evident in some equatorial Pacific locations in the NCEP2 and, to a lesser extent, CCMP2 product.

5. Wind Analysis Uncertainty Impacts on Equatorial Pacific Air-Sea CO_2 Flux

In this section we estimate the impacts that the wind biases in mean, interannual variability, and trend discussed in section 4 have on our ability to know these aspects of air-sea CO_2 flux over the equatorial Pacific. We estimate these impacts by combining the analysis wind product uncertainties revealed by the mooring wind comparison described in the section 4 with the dynamically consistent set of ΔpCO_2 and U^2 fields provided by the ESM 2G coupled model.

The ESM 2G simulation exhibits both positive and negative 25-year trends in U^2 over recent and coming decades depending on the choice of start and end year (not shown). Nevertheless, despite the simulated flip flops in U^2 25-year trend behavior, the model produces a consistently negative 25-year trend in the sea-to-air (upward) transport of carbon across the equatorial Pacific Ocean surface over this time, caused by the

simulated CO_2 partial pressure increasing faster in the atmosphere than in the near-surface equatorial Pacific Ocean. Buoy sampling the model simulation over 10 different 25-year periods spaced 1 year apart (we used 2006–2015 to mimic potential availability of MAPCO2 carbon records, which began around 2006) yields the mean value of this trend as -0.062 ± 0.01 Pg C yr^{-1} per decade, which serves as a useful reference value for the wind analysis uncertainty impacts described below.

To quantify the wind analysis uncertainty impacts, we start by subsampling the ESM 2G wind and ΔpCO_2 fields according to the availability of the high-frequency mooring wind observations. For example, starting in model year 2006, we sample the model according to the data return from the full tropical Pacific moored buoy array in place in that year, and so forth. Because the vast majority of the actual buoys do not have carbon measuring capability, this model subsampling is used to simulate the situation in which each mooring was deployed with carbon-measuring capability and provides our base-case, buoy-sampled simulation of air-sea carbon flux. To gauge the wind speed squared uncertainty effects on flux, we produce, for each analysis product considered, an alternative flux data set that is calculated using the same model ΔpCO_2 fields as in the base case but a U^2 field that has been adjusted to include the biases contained in each of the analyzed wind products as estimated based on actual mooring wind observation comparison. Taking the NCEP2 product as an example, the NCEP2-adjusted wind speed squared data set (U^2_{NCEP2*}) is calculated based on the simulated wind speed squared time series (U^2_{model}) and the observed NCEP2 biases (ε_{NCEP2})

$$U^2_{NCEP2*} = U^2_{model} + \varepsilon_{NCEP2},$$

wherein ε_{NCEP2} is the difference between the NCEP2 buoy-sampled wind speed squared (U^2_{NCEP2}) and the mooring-observed wind speed squared (U^2_{TAO}) over the 1992–2016 period

$$\varepsilon_{NCEP2} = U^2_{NCEP2} - U^2_{TAO}.$$

ε_{NCEP2} is thus a function of mooring latitude, longitude, and time (period 1992–2016). We have repeated this uncertainty-propagation approach using also the NCEP1 and CCMP2 wind products. In each case we have used 10 different model start years, from 2006 to 2015 (while ε_{NCEP2} remains unchanged but matched to a different model start year), to account for the effects of using different beginning and end dates in calculating trends and the fact that interannual and shorter timescale variability in the simulation should not be expected to be in sync with that observed. Based on these pairs (base-case-model and wind-bias-propagated) of 25-year simulated records, we calculated the mean flux difference (base-case minus bias-propagated) for each TAO mooring site (Figure 6). We also examine the degree to which introduction of the analysis product's wind speed squared biases obscures interannual variability and 25-year trend in regional air-sea CO_2 flux (Table 3).

The 25-year mean difference in flux is rather stable across the 10 different start years (standard deviation across the 10 different start year cases is less than 3% of the overall mean) and illustrated in Figure 6 using 2006 as the start year. The model-simulated net flux, averaged over the shaded region associated with each buoy in Figure 6 in this case, is +0.46 Pg C yr^{-1}, which is consistent with the current observational estimates (e.g., 0.4 Pg C yr^{-1} from Ishii et al. (2014); 0.5 Pg C yr^{-1} from Takahashi et al. (2009)) of equatorial Pacific carbon flux. The biases associated with the NCEP1 reanalysis reduce this net flux estimate by 0.18 Pg C yr^{-1}, which amounts to a reduction of about 40% from the unbiased case. By percentage, the NCEP1-associated flux reduction (−40%) is somewhat larger in magnitude than the observation-revealed deficiency in time-mean NCEP1 U^2 (−35%) that causes it. The difference (5%) in these basin-wide statistics is attributable to the nonlinear effects of spatial variability in the wind bias and ΔpCO_2 fields (e.g., wind bias effects are enhanced where ΔpCO_2 magnitudes are largest). The NCEP2 and CCMP2 products are associated with smaller U^2 biases than NCEP1 and, correspondingly, produce smaller offsets in the net air-sea flux. The wind-bias-driven flux reductions in these cases amount to 15% (NCEP2) and 6% (CCMP2) of the unbiased case and thus contribute a still substantial amount of uncertainty if accurate understanding of the carbon system is the goal. The CCMP1 biases (computed from the available 20-year rather than 25-year record; not shown for figure clarity) also produce a reduction in net flux (8%) that is comparable to but slightly larger than the CCMP2 case.

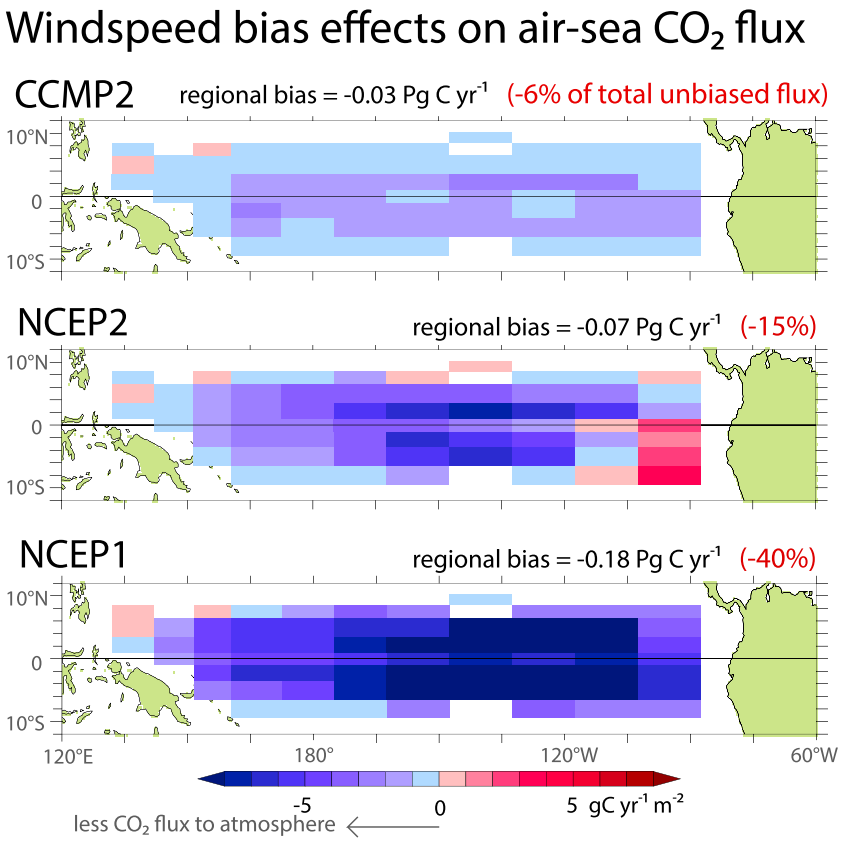

Figure 6. Impacts of the analysis product wind speed squared offsets shown in Figure 5 on 25-year mean regional carbon flux calculations.

We offer two complementary measures of the effects of wind analysis product uncertainty on our ability to estimate the interannual variability of air-sea flux over the equatorial Pacific. Each is based on the 365-day-running and all-buoy averaged difference between the unbiased and U^2-bias-propagated estimates of flux from the ESM 2G model. In one case we choose the RMSE between these two time series as the core comparison metric and in the other the standard deviation of the base-case minus bias-propagated difference (σ_Δ). The salient difference being that the RMSE accounts for any longer-term mean offset between the two cases, whereas the standard deviation approach does not. If there is little long-term offset, the two measures will be similar. If the two measures are different and the long-term offset can somehow be known and subtracted with accuracy, then σ_Δ may be the appropriate measure. Alternatively, if the offset is not stable in time, then the RMSE is the more appropriate measure of uncertainty.

Table 3
Estimated Effect of Analyzed-Product Wind Biases on Mean, Interannual Variability, and 25-year Trend in Air-Sea CO_2 Flux Over the Equatorial Pacific

	CCMP2 (1992–2016)	CCMP1 (1992–2011)	NCEP2 (1992–2016)	NCEP1 (1992–2016)
σ_Δ(Pg C yr^{-1})	0.007 ± 0.001	0.012 ± 0.001	0.023 ± 0.001	0.031 ± 0.001
σ_Δ/σ	0.106 ± 0.06	0.20 ± 0.02	0.34 ± 0.03	0.47 ± 0.03
RMSE	0.03 ± 0.001	0.04 ± 0.001	0.07 ± 0.001	0.19 ± 0.004
RMSE/σ	0.44 ± 0.02	0.56 ± 0.05	1.1 ± 0.06	2.8 ± 0.14
Mean difference (%)	−6.3 ± 0.1	−7.7 ± 0.01	−15.3 ± 0.3	−40.1 ± 0.2
Mean difference Pg C yr^{-1}	−0.030 ± 0.001	−0.036 ± 0.001	−0.070 ± 0.001	−0.18 ± 0.005
Trend difference (%)	8 ± 0.4	14 ± 1	22 ± 1	52 ± 2
Spurious trend Pg C yr^{-1} per decade	0.0063 ± 0.0003	0.013 ± 0.001	0.016 ± 0.001	0.038 ± 0.002

Note. The ± values give standard deviations produced by using 10 different model-sampling start years.

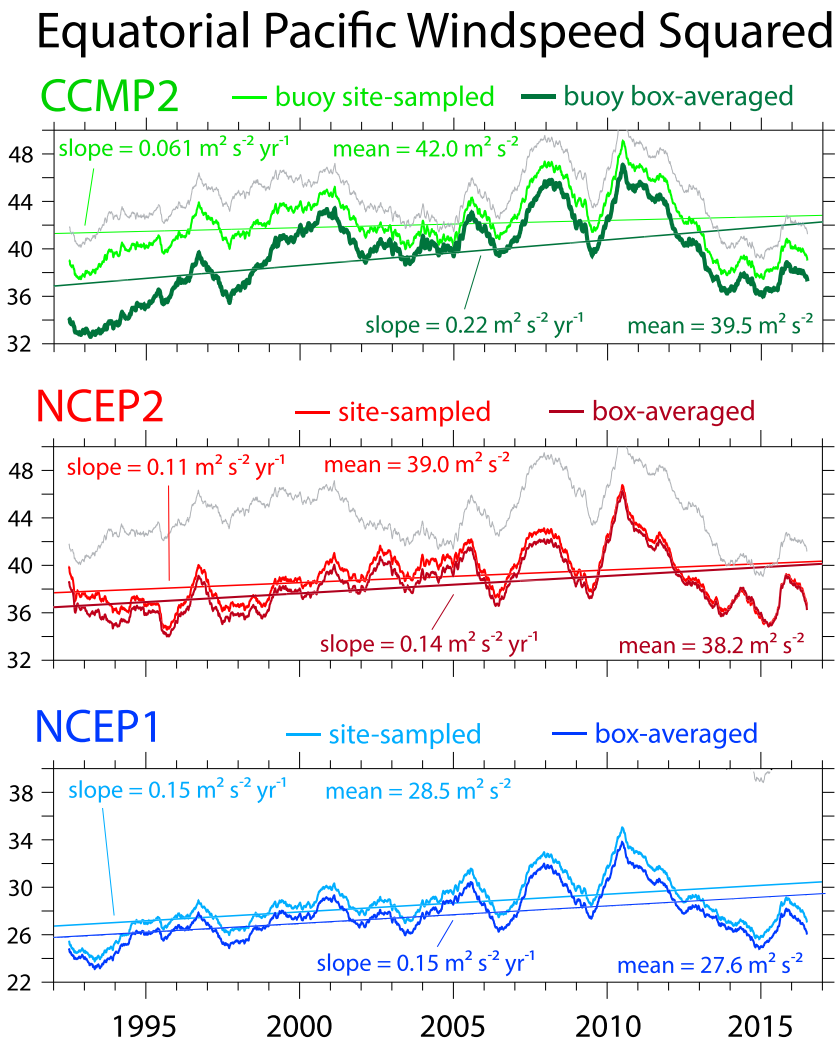

Figure 7. Ten-meter height wind speed squared, as in Figure 3, except with best fit linear trends and results from buoy box averaging (darker hues) added to the original buoy site-sampled results for comparison. Thin gray curves show the moored buoy result.

The σ_Δ values range by a factor of 4 across the analyzed wind products considered (Table 3), with CCMP2 achieving the best (0.007 ± 0.001 Pg C yr^{-1}) and NCEP1 the most deficient (0.031 ± 0.001 Pg C yr^{-1}; Table 3) result. Normalizing by the standard deviation of the simulated flux (σ_{flux}) the noise-to-signal ratios in this case range from $\sigma_\Delta/\sigma_{flux} = 0.1$ in the CCMP2 case to ~0.5 in the NCEP1 case, with the CCMP1 (0.2) and NCEP2 (0.34) results falling between these extremes. In the best (CCMP2) case, the uncertainty introduced is suggested to be small enough to permit the usefully accurate estimation of interannual timescale flux variability. In the worst case, however, the uncertainty introduced is unacceptably high for most applications; taking the observations available from the 125°W, 0°N mooring (Figure 1), for example, accepting this level of uncertainty would be roughly equivalent to desiring information about flux variability at this location but having no knowledge about the variability of surface ocean pCO_2.

Of course, the best case scenario exploits knowledge of the mean offset as is provided in this case by the mooring winds. Should this buoy information become unavailable, for example, by sections of the array dropping out from instrument failure (e.g., vandalism) and maintenance gaps, or being redeployed elsewhere, then it is unclear where knowledge of the mean offsets would come from, especially given that there are substantial changes in the decadal-averaged offsets in U^2 revealed by the buoy comparisons. For example, the CCMP2 U^2-driven flux offset averaged over the 2000–2009 period (0.024 Pg C yr^{-1}; see Figure 3), which is when the QuikScat scatterometer was available, is smaller than the average over both the prior

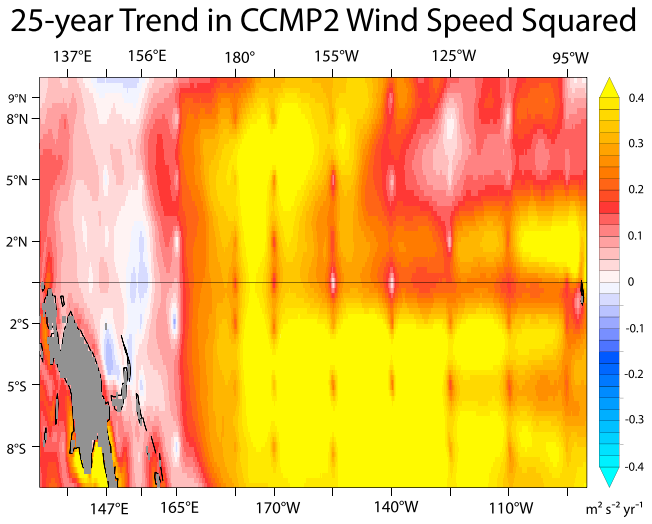

Figure 8. Slope of the best fit linear trend calculated at each grid point in the CCMP2 wind product, period 1992–2016. Tick marks along the abscissa and ordinate are placed at nominal longitudes and latitudes of the TAO/Triton moored buoy array.

(0.038 Pg C yr^{-1}) and post-2009 periods (0.027 Pg C yr^{-1}). Such variability leaves open to question the degree to which future year offsets can be approximated from previously observed behavior and suggests the RMSE as an appropriate metric. The RMSE values rank similarly to the σ_Δ values, but with a substantial increase, for example, reaching noise-to-signal (RMSE/σ) ratios of 0.44 ± 0.02 in the CCMP2 and 1.1 ± 0.06 in the NCEP2 case (Table 3), underscoring the importance that basin-wide monitoring of wind variability has on our ability to make accurate estimates of the variability of air-sea carbon flux.

In addition to the mean and interannual-timescale offsets in U^2 discussed above, there are spurious 25-year trend components contained in the analysis products considered here (20-year in the CCMP1 case) that cause spurious trends in the regional CO_2 flux estimates calculated based on them. The NCEP2 biases in U^2, which have a positive spurious trend component over the study period, cause the basin-wide net flux estimate to also have a positive (upward) spurious 25-year trend component with a magnitude of 0.016 Pg C yr^{-1} per decade based on the least squares-linear fit slope of the difference between the bias-propagated and unbiased (model simulated) regional flux. Over the model period considered, ESM 2G simulates a negative trend in flux over the equatorial Pacific basin (slope about −0.06 Pg C yr^{-1} per decade) that is caused by pCO_2 increasing faster in the model atmospheric than surface equatorial Pacific Ocean. In this scenario, the introduction of the NCEP2 biases flattens (reduces by 22%) some of the simulated negative trend. Each of the other analyzed wind data sets considered here also has a positive spurious trend component in U^2 over the study period (Table 3). The magnitude of this effect, however, varies greatly depending choice of analysis data set, with CCMP2 (in this site-sampling case) introducing the smallest and NCEP1 the largest spurious trend component in flux. The degree to which smaller spurious trend components are acceptable for useful estimation of CO_2 fluxes depends in part on the comparative rate at which the actual system is undergoing change. That our estimation of the analysis product-introduced spurious trend components in flux remains relatively stable across the 10 different start years suggests that the corresponding absolute trend values (e.g. +0.006 Pg C yr^{-1} per decade for site-sampled CCMP2) provides a useful approximation of the spurious trend that using each wind product will contribute, even in the case that other (e.g., observation-based) sources of ΔpCO_2 information are used.

6. Comparison of Buoy Site-Sampling and Buoy Box-Averaging Results

This section compares results described above based on buoy site sampling the wind products with those from the buoy box-averaging method in which the wind product grid points within rectangular regions centered on the buoy site and spanning 10–15° longitude and 2–3° latitude are averaged. This technique is motivated by results of Harrison and Luther (1990), which showed that central and western tropical Pacific Island Wind were coherent over these length scales at energetic time scales >2 days. For NCEP1, there is little appreciable difference between the 25-year trends based on these two sampling methods (slopes of best fit lines differ by <1%) and the character of interannual variability (c.f. Figure 7) remains similar by either approach. The regional time mean wind speed squared calculated from NCEP1 also remains relatively stable (<4% change between the site-sampled and box-averaged values of 28.5 and 27.6 m^2/s^2, respectively) regardless of which sampling method is chosen.

NCEP2 differences between buoy site-sampled and box-averaged mean wind speed squared values are similarly small (only 2% change between respective 39.0 and 38.2 m^2/s values). There is, however, a somewhat more noticeable effect on trend in the NCEP2 than NCEP1 case. Box sampling produces a 27% larger linear trend than site sampling, in the NCEP2 case.

Sampling method has a much larger impact on trend in the CCMP2 case than for NCEP1 and NCEP2. Whereas buoy site-sampling CCMP2 produces a 25-year trend that is relatively flat (0.061 $m^2 \cdot s^{-1}$ yr^{-1}), buoy box averaging produces a linear trend with slope of 0.22 $m^2 \cdot s^{-1}$ yr^{-1}, which is ~300% larger than

Table 4
Biases in the Equatorial Pacific Time-Mean Air-Sea Carbon Flux, As Well As 25-year Trend in Regional Air-Sea Carbon Flux Caused by Introducing the Wind Speed Squared Biases in NCEP1, NCEP2, and CCMP2 Into the ESM 2G Flux Calculation

	Buoy site sampling	Buoy box averaging
CCMP2 spurious trend (Pg C yr^{-1} per decade)	0.0063 ± 0.0003	0.029 ± 0.001
NCEP2 spurious trend	0.016 ± 0.001	0.021 ± 0.001
NCEP1 spurious trend	0.038 ± 0.002	0.039 ± 0.002
CCMP2 mean difference (Pg C yr^{-1})	−0.030 ± 0.001	−0.058 ± 0.002
NCEP2 mean difference	−0.070 ± 0.001	−0.074 ± 0.002
NCEP1 mean difference	−0.181 ± 0.005	−0.19 ± 0.006

Note. Two sets of results calculated alternatively based on buoy site sampling and buoy box averaging the analysis wind data sets are offered for comparison. Values to the right of the ± symbols indicate the standard deviation of results associated with subsampling model-simulated ΔpCO_2 fields using 10 different start years.

the CCMP2 site-sampling case and ~700% larger than the trend calculated from the moored buoy winds (0.029 $m^2 \cdot s^{-1}$ yr^{-1}). Inspection of the spatial distribution of the 1992–2016 period linear trend in CCMP2 wind speed squared (Figure 8) reveals that CCMP2 exhibits trend behavior very near the locations of the assimilated buoy observations that is substantially different from the trends found in grid boxes even just a few degrees away from the buoy sites. Regionally averaged trend statistics from CCMP2 are not representative of the buoy-observed behavior even though site-sampling CCMP2 misleadingly yields relatively good buoy versus product correspondence statistics.

Propagating the box-averaged CCMP2 wind speed squared biases through the simulated flux calculation, we find that the spurious component of regional flux in this case increases to ~0.03 Pg C yr^{-1}, which is close to five times larger than was found in the CCMP2 site-sampled case (Table 4).

7. Summary and Conclusions

Seven moored buoys deployed now for over a decade with direct carbon measuring capability in the tropical Pacific provide a unique opportunity to examine the variability of air-sea carbon flux over this region. These seven buoys are a subset of a much larger array that spans the equatorial Pacific with the minimal spacing needed to provide usefully complete information about the basin-wide variability of winds at timescales of a couple of days and longer (Chiodi & Harrison, 2017a; Luther & Harrison, 1984). The successful deployment of this array over the last 25 years means that regional wind variability from days to decades have now been resolved by this backbone component of the tropical Pacific Ocean observing system. Local wind variability down to hourly resolution is also resolved by the array based on the 10-min wind direction and wind speed averages recorded on the buoys.

Analysis of the flux records made available by the carbon-equipped subset of equatorial Pacific moorings reveals that wind variability provides the primary control on air-sea carbon flux variability measured at the six mooring sites located on the equator across the Pacific Ocean. At the 165°E, 8°S site, as well as three of the four mooring sites located farther (~20° to 50° removed) from the equator, ΔpCO_2 variability plays a larger role than wind in controlling CO_2 flux variability.

The sparseness of the available pCO_2 measurements in time and space remains a key uncertainty in estimating the actual trend in pCO_2 flux based on direct carbon observations. Winds from the full moored-buoy array, consisting of ~70 equatorial Pacific sites, however, offer a basis to estimate the effects that biases in analyzed wind products will have on direct bulk calculations of CO_2 flux.

Observations made by the full tropical Pacific moored buoy array over the 25 years from 1992 to 2016 reveal an average 10-m wind speed squared (U^2) of 44.3 m^2/s^2, with interannual variability of 2.5 m^2/s^2 and very little trend: The linear fit slope of ~0.3 m^2/s^2 per decade over the 1992–2016 period equates to a 25-year change that is less than one third of the observed interannual standard deviation.

Over the period for which the tropical Pacific mooring array has been mostly complete, each of the analyzed wind products considered here contains a spurious positive 25-year trend component. Positive spurious trend components in wind speed mask the trend in flux caused by air pCO_2 increasing faster than surface ocean pCO_2 over the equatorial Pacific. The magnitude of the spurious flux components for each analyzed wind product depended, to varying degree, on the wind product sampling method used. We considered two complementary techniques: one which mimicked the point, or site sampling offered by the buoys in actuality, and another that also took into account the behavior of the analyzed wind products near (within ~1° latitude and 5–8° longitude), but not precisely at the mooring locations. Based on results from seminal TAO/Triton design studies (e.g., Harrison & Luther, 1990) and confirmation after two decades of deployment that the array works as it was designed for providing adequate basin wide momentum flux information (Chiodi & Harrison, 2017a), we typically expect results from these two sampling approaches to be

qualitatively consistent with one another. The spurious 25-year trend component in regional air-sea carbon flux associated with using NCEP1 for wind information is 0.038 Pg C yr^{-1} per decade based on the point sampling and 0.039 Pg C yr^{-1} per decade based on averaging near the buoys. These values are within a few percent of one another yet large enough to mask over 50% of the 25-year trend in CO_2 flux simulated by the model (-0.062 ± 0.01 Pg C yr^{-1} per decade). The spurious trend in flux associated with using NCEP2 is 0.016 Pg C yr^{-1} per decade by point sampling and 0.021 Pg C yr^{-1} per decade by buoy averaging, enough to mask 20%–25% of the projected flux trend. Whether point or near-buoy averaging is used has a much larger effect on the CCMP results. By point sampling at the buoy sites, CCMP2 appears to offer improvement relative to the NCEP reanalyses, incurring a spurious positive trend in flux of only 0.0063 Pg C yr^{-1} per decade, which equates to (masking) only one tenth of the simulated regional flux trend. If, however, the nearby grid values are also considered, the spurious trend component associated with CCMP2 increases fivefold to 0.03 Pg C yr^{-1} per decade. Site sampling on its own does not offer a complete comparison with the available mooring wind observations in the CCMP case.

Recently, Wanninkhof and Triñanes (2017) used the CCMP2 wind product applied to a fixed monthly pCO_2 climatology to examine how wind speed trends in CCMP2 cause changes in the global uptake of CO_2 by the ocean. Wanninkhof and Triñanes (2017) found that CCMP2 wind speed trends over 1988–2014 were greatest in the equatorial Pacific, reportedly driving a 0.03–0.04 Pg C yr^{-1} per decade increase in regional outgassing, thereby offsetting uptake increases estimated at higher latitudes. The authors were aware of the uncertainty associated with diagnosing decadal-scale trend behavior using products like CCMP2 and reported that spot checking CCMP2 by TAO/Triton produced similar trend statistics. Although our analysis approach cannot be applied to that study's high-latitude results due to lack of a high-latitude mooring array, our analysis of the TAO/Triton region clearly shows that the trends in wind speed in CCMP2 over the full equatorial Pacific region are inconsistent with the available mooring wind observations. In fact, the biases in CCMP2 determined relative to the available mooring winds using the more regionally representative buoy box-averaging sampling strategy introduce a spurious trend component in air-sea CO_2 flux over the equatorial Pacific that roughly equates to the one reported by Wanninkhof and Triñanes (2017). We suggest that the interpretation of the regional trend in CCMP2 as being representative of the actual system deserves reconsideration. The implication is that the actual equatorial Pacific trend in CO_2 outgassing due to trends in wind is considerably smaller than their 0.03–0.04 Pg C yr^{-1} per decade range previously reported.

There are also offsets in the mean between the mooring and analyzed wind products over the equatorial Pacific: The CCMP2, NCEP2, and NCEP1 U^2 values fall short of the observed value of 44.3 m^2/s^2 by 2.2, 5.2, and 15.7 m^2/s^2, respectively, based on buoy site sampling, and 4.8, 6.1, and 16.7 m^2/s^2 based on buoy box averaging. These biases in U^2 produce negative offsets in the regional mean air-sea carbon flux of 6%–14%, 15%–18%, and 40%–43%, respectively.

For each wind product considered, we found that the biases in carbon flux caused by biases in the analyzed winds were stable across the choice of different simulated 25-year ΔpCO_2 segments. This suggests that fluxes estimated based on other sources of recent-decade ΔpCO_2 information may be usefully corrected for their wind-product-introduced biases by adjusting the analyzed winds by the available mooring wind observations.

In the other oceanic regions that do not have a mooring array designed to measure the basin-wide wind variability field, it is difficult to reliably estimate the regional biases contained in the analyzed wind products. In these cases, it is often assumed that the uncertainty associated with our knowledge of the actual system is represented by the spread between different analyzed products. Results herein, based on the selection of four analyzed wind products used most commonly in recent large-scale carbon flux studies, show that this would be an inaccurate assumption to make over the equatorial Pacific.

Monitoring and understanding the extent to which the regional carbon flux is undergoing longer-term change is key to projecting future atmospheric and oceanic concentrations. These results highlight the importance of accurate wind information in estimating the magnitude, trend, and year-to-year variability of air-sea carbon flux over the equatorial Pacific. Available wind products have significant shortcomings for this purpose, as revealed by comparison with direct wind observations from moorings. Sustained direct wind observations remain essential for accurate estimation of flux trends on interannual to multidecadal timescales.

Our finding that the observed equatorial Pacific wind speed squared behavior falls outside of the envelope of the reanalysis wind products—even though the mooring winds are available for assimilation into these products—provides a cautionary reminder that analysis products like these need to be evaluated against high-quality observations on relevant space and time scales to assess how well they represent the actual system. Understanding the uncertainties associated with synthesizing full oceanic and atmospheric pCO_2 fields based on the available observations is another important part understanding the uncertainty in our ability to monitor basin scale air-sea carbon flux. We leave complementary evaluation of observation-based pCO_2 analysis products to future work.

Acknowledgments
This study was supported by funding from the Ocean Observing and Monitoring Division of the NOAA Climate Program Office (FundRef 100007298), NOAA's Geophysical Fluid Dynamics Laboratory and Pacific Marine Environmental Laboratory (PMEL), and the Joint Institute for the Study of the Atmosphere and Ocean (JISAO). This is PMEL contribution 4795 and JISAO 2018-0163. Helpful comments on an earlier draft were provided by S. Bushinsky and H. Chen. The authors are grateful for comments from two anonymous reviewers that improved the presentation of results and helped increase the scope of this work by recommending comparison with Wanninkhof and Triñanes (2017) results. The direct carbon and wind observations, as well as wind analysis product data supporting the conclusions reached in this study, are publicly available via the websites listed in the References section. ESM 2G data are publically available through NOAA's Geophysical Fluid Dynamics Laboratory CMIP5 portal (see Reference below).

References

Atlas, R., Hoffman, R. N., Ardizzone, J., Leidner, S. M., Jusem, J. C., Smith, D. K., & Gombos, D. (2011). A cross-calibrated multiplatform ocean surface wind velocity product for meteorological and oceanographic applications. *Bulletin of the American Meteorological Society*, *92*(2), 157–174. https://doi.org/10.1175/2010BAMS2946.1

Aumont, O., & Bopp, L. (2006). Globalizing results from ocean in situ iron fertilization studies. *Global Biogeochemical Cycles*, *20*, GB2017. https://doi.org/10.1029/2005GB002591

Bakker, D. C. E., Pfeil, B., Landa, C. S., Metzl, N., O'Brien, K. M., Olsen, A., et al. (2016). A multidecade record of high-quality fCO_2 data in version 3 of the Surface Ocean CO_2 Atlas (SOCAT). *Earth System Science Data*, *8*(2), 383–413. https://doi.org/10.5194/essd-8-383-2016

Bates, N. R., & Merlivat, L. (2001). The influence of short-term wind variability on air-sea CO_2 exchange. *Geophysical Research Letters*, *28*(17), 3281–3284. https://doi.org/10.1029/2001GL012897

Blomquist, B. W., Brumer, S. E., Fairall, C. W., Huebert, B. J., Zappa, C. J., Brooks, I. M., et al. (2017). Wind speed and sea state dependencies of air-sea gas transfer: Results from the high wind speed gas exchange study (HiWinGS). *Journal of Geophysical Research: Oceans*, *122*, 8034–8062. https://doi.org/10.1002/2017JC013181

Boden, T. A., Marland, G., &Andres, R. J. (2017). Global, regional, and national fossil-fuel CO_2 emissions. Oak Ridge, TN: Carbon Dioxide Information Analysis Center, Oak Ridge National Laboratory, U.S. Department of Energy. Retrieved from http://cdiac.ornl.gov/trends/emis/overview_2014.html (Accessed 30 May 2017)

Boutin, J., Etcheto, J., Merlivat, L., & Rangama, Y. (2002). Influence of gas exchange coefficient parameterization on seasonal and regional variability of CO_2 air-sea fluxes. *Geophysical Research Letters*, *29*(8), 1182. https://doi.org/10.1029/2001GL013872

CCMP1. (2017). Cross-calibrated multi-platform ocean surface wind vector analysis, Version 1. Accessed 10 October 2017. Retrieved from ftp://podaac-ftp.jpl.nasa.gov/allData/ccmp/

CCMP2. (2017). Cross-calibrated multi-platform ocean surface wind vector analysis, Version 2. Accessed 23 August 2017. Retrieved from ftp://ftp2.remss.com/ccmp

Chiodi, A. M., & Harrison, D. E. (2017a). Simulating ENSO SSTA from TAO/TRITON winds: The impacts of 20 years of buoy observations in the Pacific waveguide and comparison with reanalysis products. *Journal of Climate*, *30*(3), 1041–1059. https://doi.org/10.1175/JCLI-D-15-0865.1

Chiodi, A. M., & Harrison, D. E. (2017b). Observed El Niño SSTA development and the effects of easterly and westerly wind events in 2014/2015. *Journal of Climate*, *30*(4), 1505–1519. https://doi.org/10.1175/JCLI-D-16-0385.1

Cronin, M. F., Fairall, C. W., & McPhaden, M. J. (2006). An assessment of buoy-derived and numerical weather prediction surface heat fluxes in the tropical Pacific. *Journal of Geophysical Research*, *111*, C06038. https://doi.org/10.1029/2005JC003324

Dee, D. P., Uppala, S. M., Simmons, A. J., Berrisford, P., Poli, P., Kobayashi, S., et al. (2011). The ERA-Interim reanalysis: Configuration and performance of the data assimilation system. *Quarterly Journal of the Royal Meteorological Society*, *137*(656), 553–597. https://doi.org/10.1002/qj.828

Doney, S. C., Lima, I., Feely, R. A., Glover, D. M., Lindsay, K., Mahowal, N., et al. (2009). Mechanisms governing interannual variability in the upper ocean inorganic carbon system and air-sea CO_2 fluxes: Physical climate and atmospheric dust. *Deep Sea Research Part II: Topical Studies in Oceanography*, *56*(8-10), 640–655. https://doi.org/10.1016/j.dsr2.2008.12.006

Dunne, J. P., Armstrong, R. A., Gnanadesikan, A., & Sarmiento, J. L. (2005). Empirical and mechanistic models for particle export ratio. *Global Biogeochemical Cycles*, *19*, GB4026. https://doi.org/10.1029/2004GB002390

Dunne, J. P., Gnanadesikan, A., Sarmiento, J. L., & Slater, R. D. (2010). Technical description of the prototype version (v0) of Tracers of Phytoplankton with Allometric Zooplankton (TOPAZ) ocean biogeochemical model as used in the Princeton IFMIP model. *Biogeosciences*, *7*(11), 3593. https://doi.org/10.5194/bg-7-3593-2010–3624

Dunne, J. P., John, J. G., Adcroft, A., Griffies, S. M., Hallberg, R., Shevliakova, E., et al. (2012). GFDL's ESM 2 global coupled climate-carbon Earth System Models. Part I: Physical formulation and baseline simulation characteristics. *Journal of Climate*, *25*(19), 6646–6665. https://doi.org/10.1175/JCLI-D-11-00560.1

Dunne, J. P., John, J. G., Shevliakova, E., Stouffer, R. J., Krasting, J. P., Malyshev, S., et al. (2013). GFDL's ESM 2 global coupled climate-carbon Earth System Models. Part II: Carbon system formulation and baseline simulation characteristics. *Journal of Climate*, *26*(7), 2247–2267. https://doi.org/10.1175/JCLI-D-12-00150.1

ESM 2G (2017). GFDL Earth System Model Version 2, employed with Generalized Ocean Layer Dynamics for the 5th Coupled Model Intercomparison Project (CMIP5). Accessed by AMC 26 July 2017. Retrieved from http://nomads.gfdl.noaa.gov:8080/DataPortal/cmip5.jsp

Fairall, C. W., Bradley, E. F., Hare, J. E., Grachev, A. A., & Edson, J. B. (2003). Bulk parameterization of air–sea fluxes: Updates and verification for the COARE algorithm. *Journal of Climate*, *16*, 571–591. https://doi.org/10.1175/1520-0442(2003)016<0571:BPOASF>2.0.CO;2

Fassbender, A. J., Sabine, C. L., Cronin, M. F., & Sutton, A. J. (2017). Mixed-layer carbon cycling at the Kuroshio Extension Observatory. *Global Biogeochemical Cycles*, *31*, 272–288. https://doi.org/10.1002/2016GB005547

Feely, R. A., Boutin, J., Cosca, C. E., Dandonneau, Y., Etcheto, J., Inoue, H. Y., et al. (2002). Seasonal and interannual variability of CO_2 in the equatorial Pacific. *Deep Sea Research Part II: Topical Studies in Oceanography*, *49*(13-14), 2443–2469. https://doi.org/10.1016/S0967-0645(02)00044-9

Feely, R. A., Takahashi, T., Wanninkhof, R., McPhaden, M. J., Cosca, C. E., Sutherland, S. C., & Carr, M.-E. (2006). Decadal variability of the air-sea CO_2 fluxes in the equatorial Pacific Ocean. *Journal of Geophysical Research*, *111*, C08S90. https://doi.org/10.1029/2005JC003129

Geider, R. J., MacIntyre, H. L., & Kana, T. M. (1997). A dynamic model of phytoplankton growth and acclimation: Responses of the balanced growth rate and chlorophyll *a*—Carbon ratio to light, nutrient-limitation and temperature. *Marine Ecology Progress Series*, *148*, 187–200.

GLOBALVIEW-CO2 (2011). GLOBALVIEW-CO_2: Cooperative Atmospheric Data Integration Project-Carbon Dioxide. CD-ROM, NOAA ESRL, Boulder, Colorado [Also available on Internet via anonymous FTP to ftp.cmdl.noaa.gov, Path: ccg/co2/GLOBALVIEW]. See version history (www.esrl.noaa.gov/gmd/ccgg/globalview/co2/co2_version.html)

Hallberg, R. (1995). Some aspects of the circulation in ocean basins with isopycnals intersecting the sloping boundaries. (PhD thesis, 244 pp.). University of Washington. Retrieved from University Microfilms, Ann Arbor, MI.

Hallberg, R. (2003). The suitability of large-scale ocean models for adapting parameterizations of boundary mixing and a description of a refined bulk mixed layer model. Near-Boundary Processes and Their Parameterization: Proceedings of the 13th 'Aha Huliko'a Hawaiian Winter Workshop (pp. 187–203). University of Hawaii at Manoa, Honolulu, HI.

Harrison, D. E., & Chiodi, A. M. (2015). Multi-decadal variability and trends in the El Niño-Southern Oscillation and tropical Pacific fisheries implications. *Deep Sea Research Part II: Topical Studies in Oceanography*, *113*, 9–21. https://doi.org/10.1016/j.dsr2.2013.12.020

Harrison, D. E., & Luther, D. S. (1990). Surface winds from tropical Pacific islands—Climatological statistics. *Journal of Climate*, *3*, 251–271.

Henson, S. A., Dunne, J. P., & Sarmiento, J. L. (2009). Decadal variability in North Atlantic phytoplankton blooms. *Journal of Geophysical Research*, *114*, C04013. https://doi.org/10.1029/2008JC005139

Ho, D. T., Law, C. S., Smith, M. J., Schlosser, P., Harvey, M., & Hill, P. (2006). Measurements of air–sea gas exchange at high wind speeds in the Southern Ocean: Implications for global parameterizations. *Geophysical ResearchLetters*, *33*, 16611. https://doi.org/10.1029/2006GL026817

Ishii, M., Feely, R. A., Rodgers, K. B., Park, G.-H., Wanninkhof, R., Sasano, D., et al. (2014). Air-sea CO_2 flux in the Pacific Ocean for the period 1990–2009. *Biogeosciences*, *11*(3), 709–734. https://doi.org/10.5194/bg-11-709-2014

Kalnay, E., Kanamitsu, M., Kistler, R., Collins, W., Deaven, D., Gandin, L., et al. (1996). The NCEP/NCAR 40-year reanalysis project. *Bulletin of the American Meteorological Society*, *77*(3), 437–471. https://doi.org/10.1175/1520-0477(1996)077<0437:TNYRP>2.0.CO;2

Kanamitsu, M., Ebisuzaki, W., Woollen, J., Yang, S.-K., Hnilo, J. J., Fiorino, M., & Potter, G. L. (2002). NCEP-DOE AMIP-II Reanalysis (R-2). *Bulletin of the American Meteorological Society*, *83*, 1631–1643

Key, R. M., Kozyr, A., Sabine, C. L., Lee, K., Wanninkhof, R., Bullister, J. L., et al. (2004). A global ocean carbon climatology: Results from Global Data Analysis Project (GLODAP). *Global Biogeochemical Cycles*, *18*, GB4031. https://doi.org/10.1029/2004GB002247

Law, R. M., Ziehn, T., Matear, R. J., Lenton, A., Chamberlain, M. A., Stevens, L. E., et al. (2017). The carbon cycle in the Australian Community Climate and Earth System Simulator (ACCESS-ESM 1)—–Part 1: Model description and pre-industrial simulation. *Geoscientific Model Development*, *10*(7), 2567–2590. https://doi.org/10.5194/gmd-10-2567-2017

Le Quéré, C., Andrew, R. M., Friedlingstein, P., Sitch, S., Pongratz, J., Manning, A. C., et al. (2018). Global carbon budget 2017. *Earth System Science Data*, *10*(1), 405–448. https://doi.org/10.5194/essd-10-405-2018

Le Quéré, C., Takahashi, T., Buitenhuis, E. T., Rödenbeck, C., & Sutherland, S. C. (2010). Impact of climate change and variability on the global oceanic sink of CO_2. *Global Biogeochemical Cycles*, *24*, GB4007. https://doi.org/10.1029/2009GB003599

Leith, C. E. (1973). The standard error of time-averaged estimates of climatic means. *Journal of Applied Meteorology*, *12*, 1066–1069.

Liss, P. S., & Merlivat, L. (1986). Air-sea gas exchange rates: Introduction and synthesis. In P. Buat-Menard (Ed.), *The role of air-sea gas exchange in geochemical cycling* (pp. 113–127). Dordrecht, Holland: D. Reidel Publishing Co.

Lovenduski, N. S., McKinley, G., Fay, A. R., Lindsay, K., & Long, M. C. (2016). Partitioning uncertainty in ocean carbon uptake projections: Internal variability, emission scenario, and model structure. *Global Biogeochemical Cycles*, *30*, 1276–1287. https://doi.org/10.1002/2016GB005426

Luther, D. S., & Harrison, D. E. (1984). Observing long-period fluctuations of surface winds in the tropical Pacific: Initial results from island data. *Monthly Weather Review*, *112*, 285–302.

MAP CO2 (2017). Moored autonomous pCO_2 system data. Accessed 14 June 2017. Retrieved from https://www.nodc.noaa.gov/ocads/oceans/Moorings/

McGillis, W. R., Edson, J. B., Ware, J. D., Dacey, J. W. H., Hare, J. E., Fairall, C. W., & Wanninkhof, R. (2001). Carbon dioxide flux techniques performed during GasEx-98. *Marine Chemistry*, *75*, 267–280. https://doi.org/10.1016/S0304-4203(01)00042-1

McGregor, S., Sen Gupta, A., Dommenget, D., Lee, T., McPhaden, M. J., & Kessler, W. S. (2017). Factors influencing the skill of synthesized satellite wind products in the tropical Pacific. *Journal of Geophysical Research: Oceans*, *122*, 1072–1089. https://doi.org/10.1002/2016JC012340

McKinley, G. A., Follows, M. J., & Marshall, J. (2004). Mechanisms of air-sea CO_2 flux variability in the equatorial Pacific and the North Atlantic. *Global Biogeochemical Cycles*, *18*, GB2011. https://doi.org/10.1029/2003GB002179

Mears, C. A., Smith, D. K., & Wentz, F. (2001). Comparison of special sensor microwave imager and buoy-measured wind speeds from 1987 to 1997. *Journal of Geophysical Research*, *106*(C6), 11,719–11,729.

Naegler, T. (2009). Reconciliation of excess ^{14}C-constrained global CO_2 piston velocity estimates. *Tellus Series B: Chemical and Physical Meteorology*, *61*, 372–384. https://doi.org/10.1111/j.1600-0889.2008.00408.x

NCEP1(1996). NCEP/NCAR Reanalysis. NOAA/OAR/ESRL PSD. Accessed 15 April 2018. Retrieved from http://www.esrl.noaa.gov/psd/data/gridded/data.ncep.reanalysis.html

NCEP2(2002). NCEP/DOE Reanalysis 2. NOAA/OAR/ESRL PSD. Accessed 15 April 2018. Retrieved from http://www.esrl.noaa.gov/psd/data/gridded/data.ncep.reanalysis2.html

Nightingale, P. D., Malin, G., Law, C. S., Watson, A. J., Liss, P. S., Liddicoat, M. I., et al. (2000). In situ evaluation of air–sea gas exchange parameterizations using novel conservative and volatile tracers. *Global Biogeochemical Cycles*, *14*(1), 373–387. https://doi.org/10.1029/1999GB900091

Orr, J. C., Najjar, R. G., Aumont, O., Bopp, L., Bullister, J. L., Danabasoglu, G., et al. (2017). Biogeochemical protocols and diagnostics for the CMIP6 Ocean Model Intercomparison Project (OMIP). *Geoscientific Model Development*, *10*(6), 2169–2199. https://doi.org/10.5194/gmd-10-2169-2017

Otero, P., Padin, X. A., Ruiz-Villareal, M., García-García, L. M., Ríos, A. F., & Pérez, F. F. (2013). Net sea-air CO_2 flux uncertainties in the Bay of Biscay based on the choice of wind speed products and gas transfer parameterizations. *Biogeosciences*, *10*, 2993–3005. https://doi.org/10.5194/bg-10-2993-2013

Park, G.-H., Wanninkhof, R., Doney, S. C., Takahashi, T., Lee, K., Feely, R. A., et al. (2010). Variability of global net sea–air CO_2 fluxes over the last three decades using empirical relationships. *Tellus Series B: Chemical and Physical Meteorology*, *62*(5), 352–368. https://doi.org/10.1111/j.1600-0889.2010.00498.x

Peixoto, J. P., & Oort, A. H. (1992). *Physics of climate* (p. 520). Melville, New York: American Institute of Physics.

Rödenbeck, C., Bakker, D. C. E., Gruber, N., Iida, Y., Jacobson, A. R., Jones, S., et al. (2015). Data-based estimates of the ocean carbon sink variability—First results of the Surface Ocean pCO_2 Mapping intercomparison (SOCOM). *Biogeosciences*, *12*(23), 7251–7278. https://doi.org/10.5194/bg-12-7251-2015

Roobaert, A., Laruelle, G. G., Landschützer, P., & Regnier, P. (2018). Uncertainty in the global oceanic CO2 uptake induced by wind forcing: quantification and spatial analysis. *Biogeosciences*, *15*, 1701–1720. https://doi.org/10.5194/bg-15-1701-2018

Sarmiento, J. L., Gloor, M., Gruber, N., Beaulieu, C., Jacobson, A. R., Fletcher, S. E. M., et al. (2010). Trends and regional distributions of land and ocean carbon sinks. *Biogeosciences*, *7*(8), 2351–2367. https://doi.org/10.5194/bg-7-2351-2010

Smethie, W. M. Jr., Takahashi, T. T., Chipman, D. W., & Ledwell, J. R. (1985). Gas exchange and CO_2 flux in the tropical Atlantic Ocean determined from ^{222}Rn and pCO_2 measurements. *Journal of Geophysical Research*, *90*, 7005–7022. https://doi.org/10.1029/JC090iC04p07005

Sutton, A. J., Sabine, C. L., Maenner-Jones, S., Lawrence-Slavas, N., Meinig, C., Feely, R. A., et al. (2014). A high-frequency atmospheric and seawater pCO_2 data set from 14 open-ocean sites using a moored autonomous system. *Earth System Science Data*, *6*(2), 353–366. https://doi.org/10.5194/essd-6-353-2014

Sutton, A. J., Wanninkhof, R., Sabine, C. L., Feely, R. A., Cronin, M. F., & Weller, R. A. (2017). Variability and trends in surface seawater pCO_2 and CO_2 flux in the Pacific Ocean. *Geophysical ResearchLetters*, *44*, 5627–5636. https://doi.org/10.1002/2017GL073814

Sweeney, C., Gloor, E., Jacobson, A. R., Key, R. M., McKinley, G., Sarmiento, J. L., & Wanninkhof, R. (2007). Constraining global air-sea gas exchange for CO_2 with recent bomb ^{14}C measurements. *Global Biogeochemical Cycles*, *21*, GB2015. https://doi.org/10.1029/2006GB002784

Takahashi, T., Sutherland, S. C., Wanninkhof, R., Sweeney, C., Feely, R. A., Chipman, D. W., et al. (2009). Climatological mean and decadal change in surface ocean pCO_2, and net sea–air CO_2 flux over the global oceans. *Deep Sea Research Part II: Topical Studies in Oceanography*, *56*(8-10), 554–577. https://doi.org/10.1016/j.dsr2.2008.12.009

TAO (1992). Tropical Atmosphere Ocean/Triangle Trans-Ocean buoy Network. Last accessed 16 July 2018. Retrieved from https://www.pmel.noaa.gov/tao/drupal/disdel/taoftp_access.html

Taylor, K. E., Stouffer, R. J., & Meehl, G. A. (2012). An overview of CMIP5 and the experiment design. *Bulletin of the American Meteorological Society*, *93*, 485–498. https://doi.org/10.1175/BAMS-D-11-00094.1

Thompson, L., Kelly, K. A., Darr, D., & Hallberg, R. (2003). Buoyancy and mixed-layer effects on the sea surface height response in an isopycnal model of the North Pacific. *Journal of Physical Oceanography*, *32*, 3657–3670.

Wallcraft, A. J., Kara, A. B., Baron, C. N., Metzger, E. J., Pauley, R. L., & Bourassa, M. A. (2009). Comparisons of monthly mean 10 m wind speeds from satellites and NWP products over the global ocean. *Journal of Geophysical Research*, *114*, D16109. https://doi.org/10.1029/2008JD011696

Wanninkhof, R. (1992). Relationship between gas exchange and wind speed over the ocean. *Journal of Geophysical Research*, *97*, 7373–7381. https://doi.org/10.1029/92JC00188

Wanninkhof, R. (2014). Relationship between wind speed and gas exchange over the ocean revisited. *Limnology and Oceanography: Methods*, *12*, 351–362.

Wanninkhof, R., Park, G.-H., Takahashi, T., Sweeney, C., Feely, R., Nojiri, Y., et al. (2013). Global ocean carbon uptake: Magnitude, variability and trends. *Biogeosciences*, *10*(3), 1983–2000. https://doi.org/10.5194/bg-10-1983-2013

Wanninkhof, R., & Triñanes, J. (2017). The impact of changing wind speeds on gas transfer and its effect on global air-sea CO_2 fluxes. *Global Biogeochemical Cycles*, *31*, 961–974. https://doi.org/10.1002/2016GB005592

Weiss, R. F. (1974). Carbon dioxide in water and seawater: The solubility of a non-ideal gas. *Marine Chemistry*, *2*(3), 203–215. https://doi.org/10.1016/0304-4203(74)90015-2